Article:
Bialic-Murphy, L., McElderry, R.M., Esquivel-Muelbert, A. et al. (115 more authors) (2024) The pace of life for forest trees. Science, 386 (6717). pp. 92-98. ISSN 0036-8075

https://doi.org/10.1126/science.adk9616

Title: The pace of life for forest trees

Lalasia Bialic-Murphy[1], Robert M. McElderry[1,2], Adriane Esquivel-Muelbert[3], Johan van den Hoogen[1], Pieter A. Zuidema[4], Oliver L. Phillips[5], Edmar Almeida de Oliveira[6], Patricia Alvarez Loayza[7], Esteban Alvarez-Davila[8], Luciana F. Alves[9], Vinícius Andrade Maia[10], Simone Aparecida Vieira[11], Lidiany Carolina Arantes da Silva[10], Alejandro Araujo-Murakami[12], Eric Arets[13], Julen Astigarraga[14], Fabrício Baccaro[15], Timothy Baker[5], Olaf Banki[16], Jorcely Barroso[17], Lilian Blanc[18], Damien Bonal[19], Frans Bongers[20], Kauane Maiara Bordin[21], Roel Brienen[5], Marcelo Brilhante de Medeiros[22], José Luís Camargo[23], Felipe Carvalho Araújo [10], Carolina V. Castilho[24], Wendeson Castro[25], Victor Chama Moscoso[26], James Comiskey[27,28], Flavia Costa[29], Sandra Cristina Müller [21], Everton Cristo de Almeida[30], Lola da Costa[31], Vitor de Andrade Kamimura[32], Fernanda de Oliveira[10], Jhon del Aguila Pasquel[33,34], Géraldine Derroire[35], Kyle Dexter[36], Anthony Di Fiore[37,38], Louis Duchesne[39], Thaise Emílio [40]†, Camila Laís Farrapo[10], Sophie Fauset[41], Federick C. Draper[42], Ted R. Feldpausch[43], Rafael Flora Ramos[44], Valeria Forni Martins[45,21], Marcelo Fragomeni Simon[46], Miguel Gama Reis[10], Angelo Gilberto Manzatto[47], Bruno Herault[48,18], Rafael Herrera[49], Eurídice Honorio Coronado[50], Robert Howe[51], Isau Huamantupa-Chuquimaco[52], Walter Huaraca Huasco[53], Katia Janaina Zanini[21], Carlos Joly[54], Timothy Killeen[55], Joice Klipel[21]†, Susan G. Laurance[56], William F. Laurance[56], Marco Aurélio Leite Fontes[10], Wilmar Lopez Oviedo[57], William E. Magnusson[58], Rubens Manoel dos Santos[10], Jose Luis Marcelo Peña [59], Karla Maria Pedra de Abreu[60], Beatriz Marimon[61], Ben Hur Marimon Junior[6], Karina Melgaço[62]†, Omar Aurelio Melo Cruz[63], Casimiro Mendoza[64], Abel Monteagudo-Mendoza[65], Paulo S. Morandi[6], Fernanda Moreira Gianasi[10], Henrique Nascimento[66], Marcelo Nascimento[67], David Neill[68], Walter Palacios[69], Nadir C. Pallqui Camacho[5], Guido Pardo[70], R. Toby Pennington[71,72], Maria Cristina Peñuela-Mora[73], Nigel C.A. Pitman[74], Lourens Poorter[4], Adriana Prieto Cruz[75], Hirma Ramírez-Angulo[76], Simone Matias Reis[77,6], Zorayda Restrepo Correa[78], Carlos Reynel Rodriguez[79], Agustín Rudas Lleras[80], Flavio A. M. Santos[54], Rodrigo Scarton Bergamin[81], Juliana Schietti[15], Gustavo Schwartz[82], Julio Serrano[83], André Maciel Silva-Sene[10], Marcos Silveira[84], Juliana Stropp[85], Hans ter Steege[16], John Terborgh[86], Mathias W. Tobler[87], Luis Valenzuela Gamarra[55], Peter J. van de Meer[88], Geertje van der Heijden[89], Rodolfo Vasquez[90], Emilio Vilanova[91], Vincent Antoine Vos[92], Amy Wolf[93], Christopher W. Woodall[94], Verginia Wortel[95], Joeri A. Zwerts[96], Thomas A.M. Pugh[97,3], Thomas W. Crowther[1]

Affiliations:

[1] Institute of Integrative Biology, ETH Zurich (Swiss Federal Institute of Technology), 8092 Zurich, Switzerland
[2] Forest Health and Biotic Interactions, Swiss Federal Research Institute WSL, 8903 Birmensdorf, Switzerland
[3] Birmingham Institute of Forest Research (BIRoR), University of Birmingham, Birnmingham, UK
[4] Forest Ecology and Forest Management group, Wageningen University & Research, Wageningen, The Netherlands
[5] School of Geography, University of Leeds, Leeds, UK
[6] Universidade do Estado de Mato Grosso (Unemat) - Pós-Graduação em Ecologia e Conservação, Nova Xavantina-MT, Brasi
[7] Nicholas School of the Environment, Duke University, Durham, NC, USA
[8] Escuela de Ciencias Agrícola, Universidad Nacional Abierta y a Distancia de Colombia
[9] Center for Tropical Research, Institute of the Environment and Sustainability, University of California ,Äì Los Angeles, Los Angeles, CA 90095, USA
[10] Universidade Federal de Lavras
[11] Universidade Estadual de Campinas, Brazil
[12] Museo de Historia Natural Noel Kempff Mercado, Universidad Autónoma Gabriel René Moreno, Santa Cruz, Bolivia
[13] Wageningen Environmental Research, Wageningen University & Research, Wageningen, The Netherlands
[14] Universidad de Alcalá, Department of Life Sciences, Forest Ecology and Restoration Group (FORECO), Alcalá de Henares, Spain
[15] Universidade Federal do Amazonas
[16] Naturalis Biodiversity Center, Leiden, The Netherlands
[17] Laboratório de Ciências Florestais. Universidade Federal do Acre, campus de Cruzeiro do Sul, Acre. Brazil
[18] Forêts et Sociétés, Univ Montpellier, CIRAD, Montpellier, France
[19] Université de Lorraine, AgroParisTech, INRAE, UMR Silva, 54000 Nancy, France
[20] Department of Environmental Sciences, Wageningen University & Research, Wageningen, The Netherlands
[21] Plant Ecology Lab, Ecology Department, Universidade Federal do Rio Grande do Sul, Porto Alegre, Brazil
[22] Embrapa Genetic Resources and Biotechnology

[23] Biological Dynamics of Forest Project - National Institute for Amazonian Research (BDFFP-INPA), Manaus Brazil
[24] Embrapa Roraima
[25] Centro de Ciências Biológicas e da Natureza, Universidade Federal do Acre, Rio Branco, Acre, Brasil
[26] Universidad Nacional de San Antonio Abad del Cusco
[27] Inventory and Monitoring Program, National Park Service
[28] Smithsonian Institution
[29] Coordenação de Pesquisas em Biodiversidade, Instituto Nacional de Pesquisas da Amazônia, Av Andre Araujo 2936, CEP 69067-375, Manaus, Brasil
[30] Universidade Federal do Oeste do Pará (UFOPA). Instituto de Biodiversidade e Florestas (IBEF). Rua Vera Paz, s/n, bairro Salé, Santarém, Pará, Brasil
[31] Universidade Federal do Oeste do Pará (UFOPA). Instituto de Biodiversidade e Florestas (IBEF). Rua Vera Paz, s/n, bairro Salé, Santarém, Pará, Brasil
[32] Instituto Tecnológico Vale (ITV), R. Boaventura da Silva, 955, 66055–090, Belém, Pará, Brazil 33 Instituto de Investigaciones de la Amazonia Peruana, Iquitos, Peru
[34] Universidad Nacional de la Amazonia Peruana, Iquitos, Peru
[35] Cirad, UMR EcoFoG (AgroParistech, CNRS, INRAE, Université des Antilles, Université de la Guyane), Campus Agronomique, Kourou, French Guiana
[36] School of GeoSciences, University of Edinburgh; Royal Botanic Garden Edinburgh
[37] Primate Molecular Ecology and Evolution Laboratory and Department of Anthropology, The University of Texas at Austin, 2201 Speedway Stop C3200, Austin, TX, 78712 USA
[38] Tiputini Biodiversity Station, College of Biological and Environmental Sciences, Universidad San Francisco de Quito, Cumbay√°, Ecuador
[39] Direction de la recherche forestière, Ministère des Ressources naturelles et des Forêts du Québec, 2700 Einstein, Quebec City, QC G1P 3W8, Canada
[40] Programa Nacional de Pós-Doutorado (PNPD), Programa de Pós-Graduação em Ecologia, Institute of Biology, University of Campinas (UNICAMP)
[41] School of Geography, Earth and Environmental Sciences, University of Plymouth
[42] School of Environmental Sciences, University of Liverpool, Liverpool, UK.
[43] Geography, Faculty of Science, Environment and Economy, University of Exeter, Exeter, UK
[44] Biology Institute, University of Campinas, 13083-862, Campinas, SP, Brazil
[45] Department of Natural Sciences, Maths, and Education, Centre for Agrarian Sciences, Universidade Federal de São Carlos (UFSCar). Araras, SP, Brazil
[46] Embrapa Recursos Genéticos e Biotecnologia, Brasília, Brazil
[47] Federal University of Rondônia (Unir-Porto Velho, RO)
[48] CIRAD, UPR Forêts et Sociétés, F-34398 Montpellier, France
[49] Instituto venezolano de Investigaciones Científicas (IVIC)
[50] School of Geography and Sustainable Development, University of St Andrews, UK
[51] Cofrin Center for Biodiversity, University of Wisconsin-Green Bay
[52] Herbario "Alwyn Gentry" (HAG); Universidad Nacional Amazónica de Madre de Dios (UNAMAD), Av. Jorge Chávez 1160. Puerto Maldonado, Madre de Dios, Perú
[53] Environmental Change Institute, School of Geography and the Environment, University of Oxford, Oxford, UK
[54] Plant Biology Department, Biology Insitute, University of Campinas
[55] Missouri Botanical Garden
[56] Centre for Environmental and Sustainability Science, College of Science and Engineering, James Cook University, Cairns, Australia
[57] Smurfit Kappa Colombia, CALLE 15 18-109 Barrio La Estancia, Yumbo, Valle del Cauca, Colombia
[58] Instituto Nacional de Pesquisas da Amazônia
[59] UNIVERSIDAD Univeridad Nacional De Juan
[60] Federal Institute of Espírito Santo, Campus de Alegre, Brazil
[61] Universidade do Estado de Mato Grosso (UNEMAT) - Programa de Pós-Graduação em Ecologia e Conservação, Nova Xavantina-MTm Brazil
[62] University of Leeds
[63] Universidad del Tolima, Ibagué, Colombia
[64] Universidad Mayor de San Simón
[65] Universidad Nacional de San Antonio Abad del Cusco, Jardin Botanico de Missouri
[66] Biodiversity Department, National Institute for the Amazon Research
[67] Laboratório de Ciências Ambientais, CBB, Universidade Estadual do Norte Fluminense Darcy Ribeiro, RJ, Brazil.

[68] Universidad Estatal Amazonica, Puyo, Pastaza, Ecuador
[69] Instituo Naional de Biodiversidad, INABIO
[70] Facultad de Ciencias Forestales, Universidad Autónoma del Beni José Ballivián, Riberalta, Beni, Bolivia
[71] Dept Geography, University of Exeter, UK and Royal Botanic Garden Edinburgh, UK
[72] Royal Botanical Garden, Edoinburgh, UK
[73] Universidad Regional Amazónica Ikiam
[74] Collections, Conservation & Research, Field Museum of Natural History, Chicago, USA
[75] ONF Andina
[76] Universidad de Los Andes. Facultad de Ciencias Forestales y Ambientales. Indefor
[77] Ciências Biológicas e da Natureza, Universidade Federal do Acre, Rio Branco, Acre, Brasil
[78] Servicios Ecosistémicos y Cambio Climático, Corporación COL-TREE, Medellin Colombia
[79] Universidad Nacional Agraria La Molina, Lima, Facultad de Ciencias Forestales
[80] Instituto de Ciencias Naturales, Universidad Nacional de Colombia
[81] School of Geography, Earth and Environmental Science, University of Birmingham, UK; Birmingham Institute of Forest Research (BIFoR), University of Birmingham, UK.
[82] Embrapa Eastern Amazon, 66095-903, Belém, PA, Brazil
[83] Universidad de Los Andes
[84] Laboratório de Botânica e Ecologia Vegetal, Centro de Ciências Biológicas e da Natureza, Universidade Federal do Acre
[85] Biogeography Department, Trier University, 54286 Trier, Germany
[86] Florida Museum of Natural History, University of Florida-Gainesville 32611 Florida, USA; School of Science and Engineering, James Cook University, Cairns, Australia
[87] San Diego Zoo Wildlife Alliance, Escondido, CA, USA
[88] Van Hall Larenstein University of Applied Sciences Velp, The Netherlands
[89] School of Geography, University of Nottingham, University Park, NG7 2RD, UK
[90] Jardín Botánico de Missouri (JBM): Oxapampa, Pasco, PE
[91] Wildlife Conservation Society (WCS), 2300 Southern Boulevard. Bronx, New York 10460, USA.
[92] Instituto de Investigaciones Forestales de la Amazonía, Universidad Autónoma del Beni José Ballivián, Riberalta, Beni, Bolivia
[93] University of Wisconsin Green Bay, Department of Natural and Applied Sciences
[94] U.S. Department of Agriculture, Forest Service, Research and Development
[95] Department of Forest Management, Centre for Agricultural Research in Suriname, CELOS, Suriname
[96] Utrecht University, Utrecht, The Netherlands
[97] Department of Physical Geography and Ecosystem Science, Lund University, Sweden

† **Present address:** TE is also affiliated with São Paulo State University (UNESP), Institute of Biosciences, Campus Rio Claro, Center for Research on Biodiversity Dynamics and Climate Change (CBioClima). KM is also affiliated with BeZero Carbon, London, England. JK is also affiliated with Leuphana University of Lüneburg, Institute of Ecology, Germany.

One Sentence Summary: The pace of life for trees varies predictably across biogeographic gradients, with important implications for modeling the forest carbon dynamics in a changing world.

***Corresponding author e-mail:** lalasia.bialicmurphy@usys.ethz.ch

Keywords: Forest ecology, life history traits, life expectancy, longevity, fast-slow continuum, trade-offs, niche differentiation, demographic diversity, tree growth stategies, demography

Abstract. Tree growth and longevity trade-offs fundamentally shape the terrestrial carbon balance. Yet, we lack a unified understanding of how such trade-offs vary across the world's forests. By mapping life history traits for a wide range of species across the Americas, we reveal considerable variation in remaining life expectancies from 10 cm in diameter (ranging from 1.3 to 3,195 years) and show that the pace of life for trees can be accurately classified into four demographic functional types. We find emergent patterns in the strength of trade-offs between growth and longevity across a temperature gradient. Furthermore, we show that the diversity of life history traits varies predictably across forest biomes, giving rise to a positive relationship between trait diversity and productivity. Our pan-latitudinal assessment provides new insights into the demographic mechanisms that govern the carbon turnover rate across forest biomes.

Introduction: The cumulative energetic investment in survival and growth from one year to the next ultimately determines an organism's overarching pace of life, including the time it takes to grow to its maximal size and its life expectancy (*1*, *2*). This fundamental relationship between energetic investments, developmental schedules, and longevity has been extensively studied for animals, showing that high resource allocation toward growth is inversely related to life expectancy and maximal body mass (*3*, *4*). Trees are also assumed to retain tightly coupled relationships between growth strategies, life expectancies, and maximal sizes (Fig. 1a) (*5*), which determine the dynamics and structure of global forests. Yet, although these life history differences fundamentally regulate how fast carbon is sequestered in different regions of the vegetation carbon pool (*6–8*), we still lack a unified understanding of the range of tree life history strategies that exist across global forests.

It is widely accepted that tree life history strategies should align along a primary axis of variation in their pace of life, ranging from fast-growing, short-lived species to slow-growing, long-lived species (i.e., fast-slow continuum and r/K selection theory) (Fig. 1a) (*5*). In this context, high energetic investment of finite resources toward fast growth is expected to come at the cost of reduced survival, which ultimately determines a species' life expectancy and maximal size (Fig. 1a) (*9–11*). Thus, it is expected that abiotic constraints (e.g. soil nutrients, water, and temperature) should strongly shape the pace of life for trees, giving rise to predictable variation in the strength of life history trade-offs across biogeographic gradients (Fig. 1b) (*12*). So far, however, the only empirical tests of these trade-offs come from tree ring data and local-scale studies from tropical ecosystems and have produced mixed results (*2*, *12–14*).

One potential challenge that can obscure predictable patterns in the pace of life for trees is that it is not only the traits that are expected to vary across environmental gradients but also the diversity of those traits. For example, strong biotic competition across tropical forests is thought to have led to high demographic niche differentiation (i.e. high demographic diversity: Fig. 1c, upper right). In contrast, resource limitations in harsh cold/dry regions are assumed to have restricted the species pool to predominantly slow-growing, long-lived species (Fig. 1c, lower left). Yet, these concepts lack empirical evidence because the extreme longevity of trees (which can live for thousands of years) has precluded our capacity to quantify the strength of tree life history trade-offs across a wide range of species, let alone characterize the diversity of life history traits across biogeographic gradients.

Here, we used the largest dataset of dynamic tree information to date and employed age-from-stage methods to calculate the mean life expectancy and maximal lifespan for a wide range of trees across the Americas (*15–17*), spanning a latitudinal gradient from Northern

Canada to Southern Brazil. This includes long-term records from an international network of researchers, including members of the Global Forest Dynamics, ForestPlots (*18*, *19*), and ForestGeo (*20–22*) networks and the United States and Canadian forest inventory programs (*23–25*). To balance this dataset across our biogeographic gradient, we randomly sub-sampled the North American plots to equal the number of point observations in Central and South America (see materials and methods), resulting in 3.2 million unique tree measurements for 1,127 species (i.e., tree size and status). Our big-data approach allowed us to test for the expectation that trees align along the fast-slow continuum (Fig. 1a, H1) and quantify if tree growth-longevity-stature relationships co-vary across soil, water, and temperature gradients (Fig. 1b, H2). Apart from species with low occurrences (< 100 observations, see materials and methods), our systematic sampling allowed us to test for the expectation that the range of life history strategies occupied by species (i.e., demographic trait diversity) varies predictably across broadscale biogeographic gradients, with harsh cold regions in the northern hemisphere restricting trees to a smaller pool of predominantly slow-growing, long-lived species (Fig. 1c, H3). Based on the well-established diversity-productivity relationship, we also expected demographic trait diversity to be positively associated with ecosystem productivity (Fig. 1c, H3).

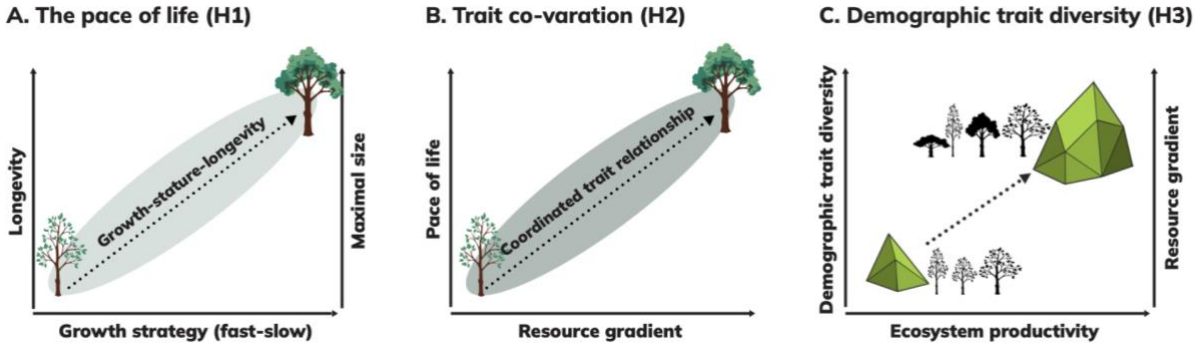

Fig. 1. Conceptual diagram of our core aims and associated hypotheses. The expectation is that trees should align along the fast-slow continuum, with fast-growing short-lived species on one end of the spectrum and slow-growing long-lived species on the other end (H1, panel **A**). Life history trait relationships should be phylogenetically conserved and should co-vary across biogeographic gradients, leading to more conservative life history strategies in low-resource environments (low soil and nutrient environments and colder temperatures) (H2, panel **B**). Lastly, we expect the range of tree life history strategies (i.e., convex-hull volume in life history trait space that is occupied by species) to vary predictably across biogeographic gradients, with demographic trait diversity being positively associated with ecosystem productivity (H3, panel **C**).

To quantify tree growth, longevity, and stature for a wide range of species across biogeographic gradients and test our three core hypotheses, we first grouped the stem-level tree data into equally sized hexagon grids (size ~ 250,000 km^2) and developed species-specific survival and growth generalized linear mixed effect models that included tree diameter at breast height (dbh) at the first census interval as a predictor variable and grid cell as a random effect (see materials and methods). We then used the survival and growth coefficients to fit size-dependent integral projection models (IPMs) and derive age-related traits from size-dependent probabilities for each species within each grid cell (see materials and methods) (*15–17*, *26–28*). IPMs dynamically integrate size-dependent variability in survival and growth as a continuous process, which allowed us to use cross-sectional data over discrete time steps to make interspecific comparisons in how many years it takes trees to attain key milestones in their life cycle. We parameterized our IPMs using methods specifically developed for trees (*27–29*). Validations of IPM model outputs, relative to tree

ring data, showed this parameterization method can provide realistic estimates of tree age demographics (*27*).

We used our species-specific IPMs and employed age-from-stage methods to calculate several quantitative measures of growth, longevity, and stature. Specifically, we calculated the number of years it takes for trees to grow from 10 to 20 cm in diameter (fig. S2, path a.2) and grow from 10 cm to the 70th quantile of their size distribution (fig. S2, path a.1) (hereafter referred to as *growth strategies*). The 10 cm in diameter lower bound threshold was chosen because it was the size at which point trees were consistently monitored across the forest networks and the 70th quantile threshold was chosen because it reflects a mature size at which point trees have approached their ultimate position in the forest. We also calculated two quantitative measures of tree longevity, including their average remaining life expectancy from 10 cm in diameter and their maximal lifespan age (95% cohort mortality from 10 cm), and a measure of maximal tree stature (size at maximal lifespan age) (fig. S2, path b) (*15–17*). These mean estimates capture the pace of life for trees (growth, longevity, and stature) based on observed climate conditions over the last century (derived from dynamical data collected between 1926-2014, see materials and methods).

Our estimates of remaining life expectancy from 10 cm dbh range from 1.2 to 3,195 years, with a mean value of 60 years in the tropics and 95 years in the extratropics (Fig 2a). This trend matches our theoretical expectation of broadscale tree life history diversification patterns (Fig. 1b) and confers with known tree longevity hot spots, whereby the oldest recorded species occur in temperate conifer and boreal forests (*12*, *30*). However, there was also considerable overlap in the range of tree life expectancies across biomes (fig S3-S4), table S2) and wide variability in how longevity relates to tree growth strategies and maximal statures (Fig. 2b, fig S3-S4, and table S2). It is important to note that remaining life expectancy from 10 cm dbh is a species-level mean estimate (i.e. is conditional on surviving to 10 cm dbh). A low life expectancy, relative to the mean number of years it takes a species to grow from 10-20 cm dbh, does not imply that no individuals will reach 20 cm dbh. Instead, it implies that less than half of the individuals will survive to that size threshold.

Tree life history strategies do not strictly follow the fast-slow continuum (H1).

To test the expectation that trees align along the fast-slow continuum (Fig. 1a, H1), we first examined univariate trait correlations and found moderate support for trade-offs between tree growth, longevity, and stature (fig. S5). For example, the number of years it takes trees to grow from 10-20 cm in diameter was positively correlated to life expectancy (Pearson correlation = 0.22) and maximal lifespan age (Pearson correlation = 0.21). Similarly, maximal tree size was positively related to life expectancy (Pearson correlation = 0.41). Interestingly, the strength of these pairwise correlations also suggests that tree age demographics do not strictly follow a single axis of variation along the fast-slow continuum (i.e., the assumption that growth is tightly coupled and inversely related to longevity and maximal stature).

To examine the multidimensionality of tree age demographics (Fig. 1A, H1), we analyzed the variance-covariance matrix of tree growth, longevity, and stature using a principal component analysis (PCA). Highly correlated traits that captured redundant trait information were excluded from the PCA (fig. S5), resulting in the inclusion of tree growth strategies (i.e., growth from 10 to 20 cm dbh and the 70th quantile of their size distribution), life expectancy from 10 cm dbh, and maximal tree size (fig. S5). The first PC axis captured 46% of the life history trait variation and was heavily weighted by tree growth dynamics (i.e., years to 20 cm

dbh and the 70th quantile size) (Fig. 2C). The PC loadings also showed that slow growth was correlated with high life expectancy and large maximal size (table S3). The second axis captured 28% of the trait variation. Interestingly, the directionality between the trait correlations flipped, whereby slow growth was negatively correlated to life expectancy and maximal size (table S3). The third axis was heavily weighted by tree life expectancy, with high life expectancy being positively related to slow growth but negatively related to tree maximal size (table S3). PCA analyses for tropical versus extratropical species retain consistent patterns in the directionality of the trait correlations among the PC axes (table S3), illustrating the modular and flexible nature of tree age demographics beyond the fast-slow continuum within and among the Northern and Southern hemispheres.

To further contextualize how the variation in tree age demographics among the PC axes shapes the overarching pace of life for trees, we used a K-means clustering algorithm to group species into core demographic functional types (see material and methods subsection 3 and fig. S6). Using this clustering algorithm, which reduces the within-group sum of squares, we found that fast-growing species aggregated into a single stature-longevity functional type (Fig. 2C-2D, cluster 1). Conversely, conservative slow-growing species formed three distinct clusters, including low, intermediate, and high stature-longevity functional types (Fig. 2C-2D, clusters 2-4). The fast-growing species cluster matches the theoretical expectation of ubiquitous resource limitations that constrain a species' ability to maintain high growth and high survival simultaneously, leading to low life expectancies and small maximal sizes (Fig. 2C-2D, cluster 1). Yet, the emergence of three distinct clusters for slow-growing species suggests conservative trees are less constrained in their pace of life. At one end of these three conservative growth trait clusters were species with high life expectancies but small maximal sizes (Fig. 2C-2D, cluster 4), and at the other end were species with low life expectancies but large maximal sizes (Fig. 2C-2D, cluster 3). Clustering analyses for tropical versus extratropical species indicate that the tropics retain the full range of demographic functional types (fig. S7, four distinct clusters), Conversely, the extratropical species group into two demographic functional types of predominantly slow-growing conservative clusters (fig. S7, two distinct clusters). Together, these results provide key insight into the core groups of demographic functional types that shape the structural complexity and dynamics of tropical versus extratropical forests.

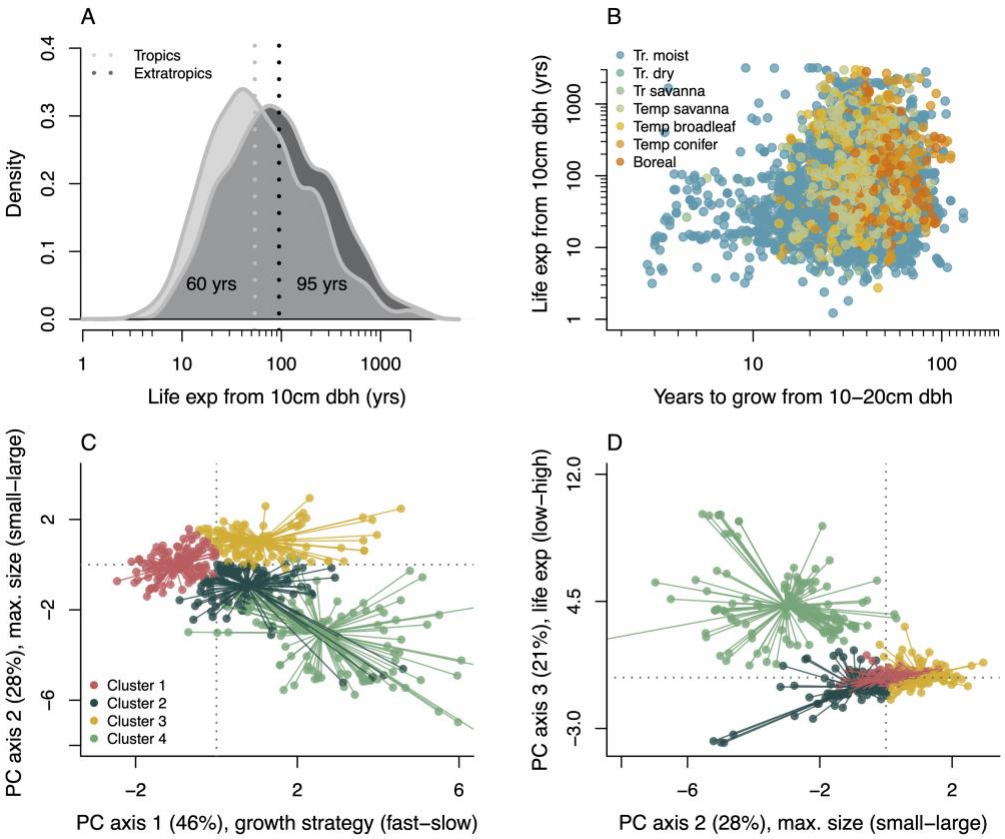

Fig. 2. Visual illustration of tree growth-longevity-stature relationships and core demographic functional types. The mean life expectancy is higher in the extratropics than in the tropics (**A**), with substantial variation between tree growth strategies and life expectancies (**B**) (N=6,847 i.e., species X grid ID). The other trait relationships are represented in fig. S8. The core growth-longevity-stature functional types are presented in **C-D**, which are determined using the K-means clustering algorithm of the life history trait PC scores. PC weights and trait correlations are reported in table S3. The frequency density **(A)** and the life history traits (**B**) are scaled by the natural log. The axes for **A-D** are scaled by the natural log. Data points are species-specific and are calculated using individual tree observations and size-dependent integral projection models (see materials and methods).

Our broadscale assessment of growth-longevity-stature relationships for a wide range of species across the Americas is consistent with trends derived from tropical forest plots, which found survival and growth rates over discrete size ranges differed substantially among species and diminished as trees attained larger sizes (*31–37*). Similarly, while tree-ring data showed that annual growth rates were negatively correlated with observed maximal ages (*12*), there was more variation in observed maximal ages for species with fast versus slow growth (*12*, *14*). Together, these emergent patterns illustrate the modular and flexible nature of trees that extend beyond the fast-slow continuum (Fig. 2C-2D, figs. S3-S4) and highlight the tremendous variation in tree life expectancies across forest biomes (Fig 2A and figs. S3-S4), with some of the oldest living species having a remaining life expectancy > 2000 years (such as *Tsuga heterophylla* and *Sequoia sempervirens*).

Building on these foundational insights from predominantly tropical ecosystems, our results provide a novel perspective that contributes to our fundamental understanding of tree age demographics. By converting survival and growth rates over species life cycles to age-based traits, our results provide insight into the time it takes trees to reach their ultimate positions in the forest and their mean age at death (e.g., life expectancy). This allowed us to quantify the pace of life for a wide range of species across the Americas and identify the core demographic functional types more directly linked to carbon turnover. The emergence of the

slow-growth short-lifespan functional trait cluster is in line with previous research from tropical forests, which showed that some short-stature trees had slow growth and low survival (*31*, *32*, *34*, *38*). This emergent trend may be an indication of maladapted species, or a mediated effect of environmental disturbance (*10*, *32*, *33*). Conversely, it could be the result of energetic investments in reproduction over species' lifespans (net reproductive rate) that we were not able to capture in our analysis (*5*, *11*, *31*, *34*). Regardless of the mechanisms, our findings provide a novel perspective on the multidimensionality of tree age demographics for a wide range of phylogenetic and geographical groups. Furthermore, our finding of emergent differences in the number of demographic functional types in the tropics versus extratropics provides novel insight into the mechanisms that shape the dynamics and structure of forests across the Americas.

Weak coordination in the strength of life history trade-offs across biogeographic gradients (H2).

To test for emergent patterns in the strength of tree life history trade-offs across biogeographic gradients (Fig. 1b, H2), we fit a multi-response Bayesian generalized mixed effect model that included the first PC axis for each of three comprehensive sets of variables related to soil, temperature, and precipitation as fixed effects and the phylogenetic relatedness as a random effect (see materials and methods, table S4, figs S6-S8) (*39*). These abiotic indexes were selected because they are known to strongly regulate photosynthetic capacity and plant growth and are commonly assumed to induce life history trade-offs. This approach allowed us to test for covariation in life history trait responses across soil, temperature, and precipitation indexes and control for the effects of phylogenetic ancestry (*40*). These soil, temperature, and precipitation variables were based on mean conditions from 1997-2013 (see materials and methods, table S4), which overlap with the time window that our dynamical tree data were collected. The expectation is that tree life history trade-offs are shaped by the shared influence of abiotic factors and phylogenetic constraints, with colder temperatures and lower resource availability pushing species toward the conservative end of the life history trait spectrum (Fig. 1b, H2).

Our results show that there is a strong relationship between temperature and tree life history traits, with colder temperatures being associated with conservative growth (β = -0.02, CI = (-0.03, -0.01)) and high life expectancies (β = -0.07, CI = (-0.05, -0.08)) (Fig. 3 and fig. S12). Conversely, our precipitation and soil indices had a weak effect on life history traits (fig. 12, table S.5). Consistent with Amazon research (*41*), we found that tree life history traits were phylogenetically conserved (Pagel's λ ranging from 0.88-0.99, fig. S14 and table S6). Yet, we also found low phenotypic correlations among our life history traits, indicating that the strength of trade-offs between tree growth, longevity, and stature do not strongly co-vary across biogeographic gradients (Fig. 1b, H2). For example, the phenotypic correlation between the number of years it takes trees to grow to 20 cm dbh and their life expectancy from 10 cm dbh was 0.18 (Fig. 3a). Together, these results show that, while tree life history traits are phylogenetically conserved (Δ DIC null model versus phylo. model = 76832), growth-longevity-stature relationships are not driven by genetic linkages or shared selective pressures that act on both traits independently over evolutionary time across broad-scale resource gradients (table S6) (*42*).

While our results offer the most comprehensive assessment of tree age demographics across broadscale resource gradients, it is important to note the data gap in the subtropics (i.e., across Mexico and northern Central America, Fig S1). This data gap could help explain the noticeable difference in the range of life history trait strategies between the North American

temperate forests (low trait variation) and South American tropical forests (high trait variation) (Fig 3B-3D and fig S1). This data gap highlights the need for increased sampling efforts in these understudied regions of the world and should be a priority of future research and funding.

Our findings are in line with trade-offs between physiological and morphological plant features linked to individual fitness and life history evolution, one reflecting leaf economic variables related to photosynthetic activity and growth potential and the other associated with morphological features related to light competition and plant height (*43–45*). Yet, similar to our results, the dominant axes of physiological and morphological plant features did not strongly co-vary across latitudinal gradients (*44*, *45*). Together, our findings and previous research suggest that organismal function that supports rapid growth is not necessarily linked to organismal function that results in lower life expectancies and small maximal sizes. These emergent patterns suggest that rapid shifts in climate conditions may have divergent effects on the relationship between biomass accumulation in tree growth and biomass retention in tree longevity, with important implications for modeling the global carbon balance in a changing world (*46*).

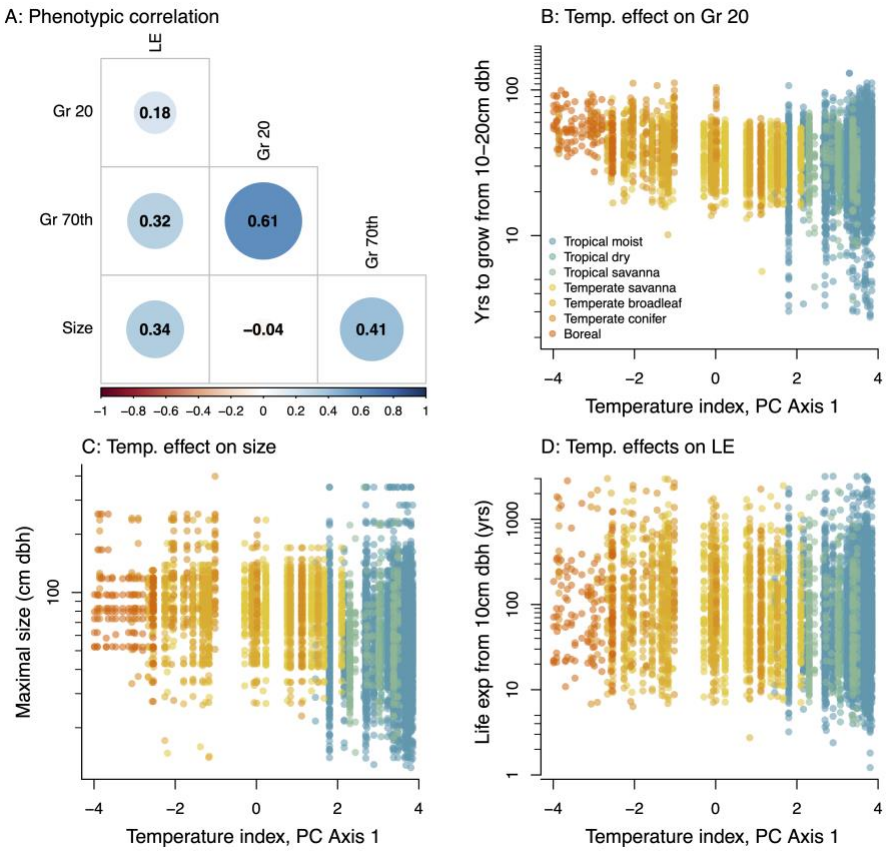

Fig. 3. Tree life history traits across our temperature index (PC axis 1 for a comprehensive list of temperature variables, see materials and methods). Overall, we found low phenotypic correlations [variance-covariance of standardized traits] among tree growth, longevity, and stature, suggesting there is weak support for coordinated trade-offs over evolutionary time (i.e., organismal function that supports conservative growth does not necessarily trade-off with organismal function needed to maintain high longevity) (**A**). We also find a strong effect of temperature on tree life history traits (panels **B-D**), with little additional variation explained by soil or precipitation (see figs. S12-S13 and table S5). The temperature gradient is derived from a principal component analysis of nine temperature variables and represents a gradient from intermediate temperatures in the tropical moist forest of the southern hemisphere to colder temperatures in the boreal north (from left to right of the x-

axis). The y-axis is scaled by the natural log. Data points are species-specific and are calculated using individual tree observations to fit size-based integral projection models for each species within each grid cell ID (total of 1,127 species and 6,847 trait values) (see materials and methods). Model coefficients of the multi-response Bayesian model are reported in fig. S12 and table S5).

Demographic diversity varies predictably across biogeographic gradients (H3).
To characterize the range of life history strategies that are expressed by trees across broadscale biogeographic gradients, we first calculated the convex-hull volume in demographic trait space within each grid cell (see materials and methods) (*47*) and compared the relationship between the demographic trait diversity of forests and well-established patterns in species richness. The convex-hull volume was calculated using the life history trait PC scores for axes 1-3, which together captured 95% of the life history trait variation. We then tested if the demographic trait diversity of forests varied predictably across biogeographic gradients, and explored potential links between demographic trait diversity and remotely sensed estimates of potential above-ground net primary productivity (NPP) (Fig. 1c, H3, see materials and methods) (*48*). The expectation is that the diversity of life history trait strategies that are expressed by trees should vary predictably across biogeographic gradients, with higher demographic diversity being positively associated with above-ground productivity.

Our results illustrate that the demographic trait diversity of forests follows well-established patterns in species richness (Fig. 4a, adj R^2 =0.65, $p < 0.001$). We also found that the demographic diversity of forests varied predictably across biogeographic gradients, with high demographic trait diversity across warm tropical forests and low diversity of predominantly slow-growing, long-lived species in the cold temperate and boreal forests (adj R^2 =0.40, $p < 0.001$, Fig. 4b and table S7). Lastly, we found a positive correlation between the demographic diversity of forests and remotely sensed estimates of ecosystem productivity (Pearson correlation = 0.71).

The emergence of a positive association between the demographic trait diversity and ecosystem productivity is in line with two non-mutually exclusive hypotheses. From an evolutionary perspective, ecosystem productivity is thought to drive species diversification and niche differentiation (*49*). Conversely, following widely established relationships between biodiversity and ecosystem function, more demographically diverse forests are commonly assumed to have access to a larger resource pool and should thus be more productive (*50*, *51*). Here, we found moderate support for both hypotheses. Specifically, we found that ecosystem productivity was predictive of demographic trait diversity across broad-scale biogeographic gradients (adj R^2 = 0.49, $p < 0.001$, Fig. 4c, table S7). At the same time, ecosystem productivity was jointly influenced by temperature (average marginal effect = 0.83, p =0.04, Fig. 4d) and demographic trait diversity (average marginal effect = 1.43, $p < 0.001$, Fig. 4d). This positive association was consistent across the tropics (adj R^2 =0.26, $p < 0.01$, table S7) and extra-tropics (adj R^2 = 0.84, $p < 0.01$, Fig. 4d, table S7). It should be noted that NPP was strongly correlated with mean annual temperature (Pearson correlation = 0.94), which did not allow us to explicitly test for the individual and combined effect of these variables on demographic trait diversity. While our broadscale analysis does not establish causality in the direction of these relationships, it does highlight the inextricable link between demographic trait diversity and ecosystem productivity across forest biomes.

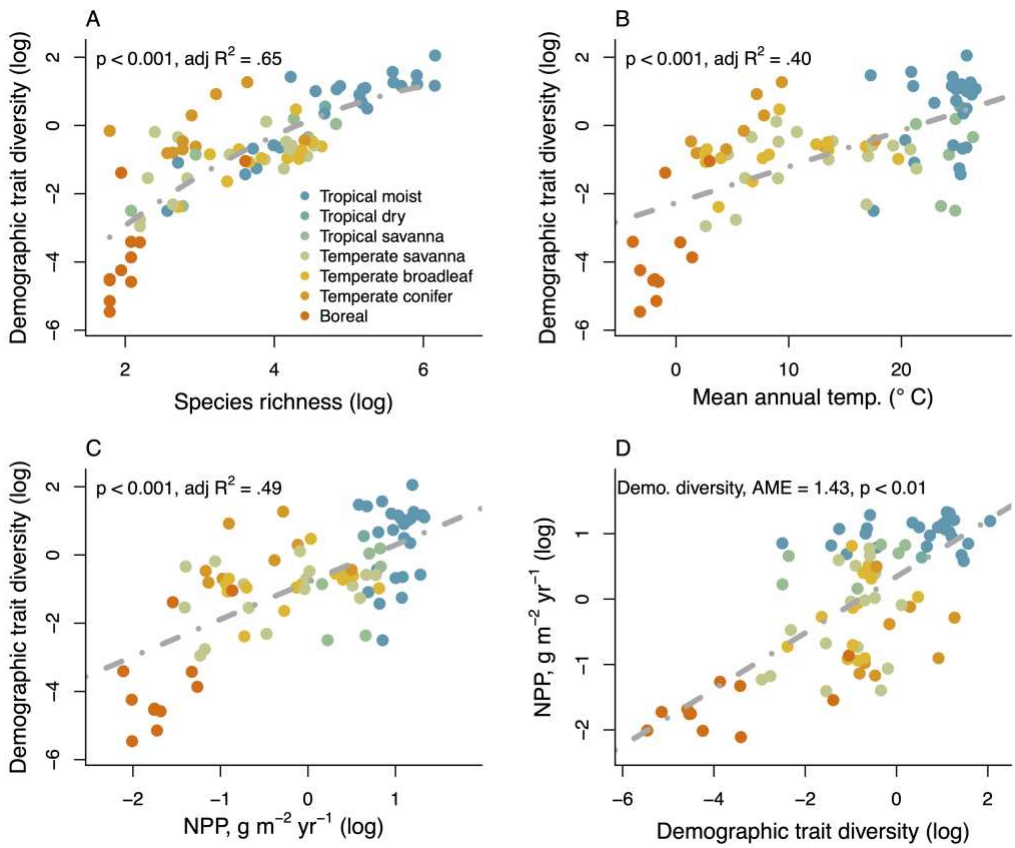

Fig. 4. The relationship between the demographic trait diversity of forests and ecosystem productivity (H3). We find that the demographic trait diversity is positively related to species richness (A), with increasing demographic trait diversity (i.e., convex-hull volume in life history trait space that is occupied by species) across a mean annual temperature gradient (B). In line with two non-mutually exclusive hypotheses in evolutionary biology and functional ecology, we find a positive association between demographic trait diversity and above-ground net primary productivity (NPP) (C and D). It is important to note that NPP was based on remotely sensed estimates and that these analyses do not establish causality in the directionality of this relationship (C and D). The fully parameterized model in panel D includes the demographic trait diversity and mean annual temperature. Demographic trait diversity and NPP were scaled to a mean of zero and a standard deviation of one. Average marginal effects (AME) represent the response per unit increase for each predictor variable.

The established association between demographic trait diversity and ecosystem productivity is in line with emergent patterns derived from tropical forest plots, which found that the demographic composition of forests was predictive of empirically derived measures of above-ground carbon dynamics (*32*). Similarly, our findings match theoretical expectations that the pace of life of organisms within a community (e.g., life expectancy and generation time) should strongly regulate the relationship between carbon turnover (ecosystem fluxes) and carbon retention (ecosystem pools) (*52*). It is important to note that the association between demographic trait diversity and ecosystem productivity was derived from multi-year averages in remotely sensed NPP from 1997-2013 and mean estimates of tree growth-longevity-stature relationships based on the current distribution of species (i.e., derived from dynamical data collected from the 1900s-2000s). This approach did not allow us to account for potential biogeographic biases in the effects of human disturbance on species diversity (i.e., between boreal and tropical forests). Yet, by quantifying the current distribution of demographic functional types across broad-scale resource gradients, our results provide a powerful backdrop for parameterizing next-generation vegetation models to simulate forest carbon turnover rates across a range of current and future conditions.

More generally, our analysis offers strong empirical support for the expectation of high demographic trait diversity in tropical forests compared to temperate and boreal forests. This multi-biome finding supports the community assembly theory of strong abiotic filtering in boreal regions, resulting in a restricted species pool of predominantly slow-growing, long-lived species (Fig. 1c, H3). This emergent pattern is congruent with known variability in physiological leaf trait characteristics across biogeographic gradients (*43–45*), with decreasing variation in leaf economic traits from lower to higher latitudes (*53*). Similarly, our results match well-established species richness–productivity relationships across global forests (*51*, *54*) and community structure-productivity relationships (*55*). Yet, while it makes intuitive sense that the demographic diversity of forest communities follows well-established patterns in species richness (*49*, *50*), our findings establish a more direct link to the demographic mechanisms that generate global variation in ecosystem carbon turnover.

Conclusion:

Our broad-scale analysis reveals the remarkable diversity of life history strategies that exist for tree species across the Americas. Weak trade-offs between tree growth, longevity, and stature across biogeographic gradients demonstrate the modular and flexible nature of trees, highlighting the diversity of evolutionary trajectories that have arisen to address the ecological puzzle of survival. In addition, from a functional perspective, we find that while acquisitive trees sequester carbon at faster rates, they also generally appear constrained to smaller maximum sizes and shorter lifespans that translate to lower carbon storage and faster carbon turnover. More importantly, we find that more demographically diverse forests tend to be more productive at the ecosystem scale across the tropics and extra-tropics. These findings have important implications for informing global restoration and conservation efforts, and for understanding the fundamental feedback between biodiversity and climate change mitigation.

References:

1. H. Caswell, *Matrix Population Models* (Sunderland: Sinauer, 2000)vol. 1.

2. C. J. E. Metcalf, C. C. Horvitz, S. Tuljapurkar, D. A. Clark, A time to grow and a time to die: a new way to analyze the dynamics of size, light, age, and death of tropical trees. *Ecology* **90**, 2766–2778 (2009).

3. J. P. de Magalhães, J. Costa, G. M. Church, An Analysis of the Relationship Between Metabolism, Developmental Schedules, and Longevity Using Phylogenetic Independent Contrasts. *J. Gerontol. Ser. A* **62**, 149–160 (2007).

4. D. E. L. Promislow, On Size and Survival: Progress and Pitfalls in the Allometry of Life Span. *J. Gerontol.* **48**, B115–B123 (1993).

5. S. C. Stearns, Trade-Offs in Life-History Evolution. *Funct. Ecol.* **3**, 259 (1989).

6. N. G. McDowell, C. D. Allen, K. Anderson-Teixeira, B. H. Aukema, B. Bond-Lamberty, L. Chini, J. S. Clark, M. Dietze, C. Grossiord, A. Hanbury-Brown, G. C. Hurtt, R. B. Jackson, D. J. Johnson, L. Kueppers, J. W. Lichstein, K. Ogle, B. Poulter, T. A. M. Pugh, R. Seidl, M. G. Turner, M. Uriarte, A. P. Walker, C. Xu, Pervasive shifts in forest dynamics in a changing world. *Science* **368**, eaaz9463 (2020).

7. U. Büntgen, P. J. Krusic, A. Piermattei, D. A. Coomes, J. Esper, V. S. Myglan, A. V. Kirdyanov, J. J. Camarero, A. Crivellaro, C. Körner, Limited capacity of tree growth to

mitigate the global greenhouse effect under predicted warming. *Nat. Commun.* **10**, 2171 (2019).

8. C. Körner, A matter of tree longevity. *Science* **355**, 130–131 (2017).

9. P. B. Reich, The world-wide 'fast-slow' plant economics spectrum: a traits manifesto. *J. Ecol.* **102**, 275–301 (2014).

10. S. E. Russo, S. M. McMahon, M. Detto, G. Ledder, S. J. Wright, R. S. Condit, S. J. Davies, P. S. Ashton, S. Bunyavejchewin, C.-H. Chang-Yang, S. Ediriweera, C. E. N. Ewango, C. Fletcher, R. B. Foster, C. V. S. Gunatilleke, I. A. U. N. Gunatilleke, T. Hart, C.-F. Hsieh, S. P. Hubbell, A. Itoh, A. R. Kassim, Y. T. Leong, Y. C. Lin, J.-R. Makana, M. Bt. Mohamad, P. Ong, A. Sugiyama, I.-F. Sun, S. Tan, J. Thompson, T. Yamakura, S. L. Yap, J. K. Zimmerman, The interspecific growth–mortality trade-off is not a general framework for tropical forest community structure. *Nat. Ecol. Evol.* **5**, 174–183 (2020).

11. R. Salguero-Gómez, O. R. Jones, E. Jongejans, S. P. Blomberg, D. J. Hodgson, C. Mbeau-Ache, P. A. Zuidema, H. de Kroon, Y. M. Buckley, Fast–slow continuum and reproductive strategies structure plant life-history variation worldwide. *Proc. Natl. Acad. Sci.* **113**, 230–235 (2016).

12. G. M. Locosselli, R. J. W. Brienen, M. de S. Leite, M. Gloor, S. Krottenthaler, A. A. de Oliveira, J. Barichivich, D. Anhuf, G. Ceccantini, J. Schöngart, M. Buckeridge, Global tree-ring analysis reveals rapid decrease in tropical tree longevity with temperature. *Proc. Natl. Acad. Sci.* **117**, 33358–33364 (2020).

13. D. A. Clark, D. B. Clark, ASSESSING THE GROWTH OF TROPICAL RAIN FOREST TREES: ISSUES FOR FOREST MODELING AND MANAGEMENT. *Ecol. Appl.* **9**, 981–997 (1999).

14. R. J. W. Brienen, L. Caldwell, L. Duchesne, S. Voelker, J. Barichivich, M. Baliva, G. Ceccantini, A. Di Filippo, S. Helama, G. M. Locosselli, L. Lopez, G. Piovesan, J. Schöngart, R. Villalba, E. Gloor, Forest carbon sink neutralized by pervasive growth-lifespan trade-offs. *Nat. Commun.* **11**, 4241 (2020).

15. M. E. Cochran, S. Ellner, Simple Methods for Calculating Age-Based Life History Parameters for Stage-Structured Populations. doi: 10.6084/M9.FIGSHARE.C.3308904 (2016).

16. S. Tuljapurkar, C. C. Horvitz, FROM STAGE TO AGE IN VARIABLE ENVIRONMENTS: LIFE EXPECTANCY AND SURVIVORSHIP. *Ecology* **87**, 1497–1509 (2006).

17. C. C. Horvitz, S. Tuljapurkar, Stage Dynamics, Period Survival, and Mortality Plateaus. *Am. Nat.* **172**, 203–215 (2008).

18. ForestPlots.net, C. Blundo, J. Carilla, R. Grau, A. Malizia, L. Malizia, O. Osinaga-Acosta, M. Bird, M. Bradford, D. Catchpole, A. Ford, A. Graham, D. Hilbert, J. Kemp, S. Laurance, W. Laurance, F. Y. Ishida, A. Marshall, C. Waite, H. Woell, J.-F. Bastin, M. Bauters, H. Beeckman, P. Boeckx, J. Bogaert, C. De Canniere, T. De Haulleville, J.-L. Doucet, O. Hardy, W. Hubau, E. Kearsley, H. Verbeeck, J. Vleminckx, S. W.

Brewer, A. Alarcón, A. Araujo-Murakami, E. Arets, L. Arroyo, E. Chavez, T. Fredericksen, R. G. Villaroel, G. G. Sibauty, T. Killeen, J. C. Licona, J. Lleigue, C. Mendoza, S. Murakami, A. P. Gutierrez, G. Pardo, M. Peña-Claros, L. Poorter, M. Toledo, J. V. Cayo, L. J. Viscarra, V. Vos, J. Ahumada, E. Almeida, J. Almeida, E. A. De Oliveira, W. A. Da Cruz, A. A. De Oliveira, F. A. Carvalho, F. A. Obermuller, A. Andrade, F. A. Carvalho, S. A. Vieira, A. C. Aquino, L. Aragão, A. C. Araújo, M. A. Assis, J. A. M. A. Gomes, F. Baccaro, P. B. De Camargo, P. Barni, J. Barroso, L. C. Bernacci, K. Bordin, M. B. De Medeiros, I. Broggio, J. L. Camargo, D. Cardoso, M. A. Carniello, A. L. C. Rochelle, C. Castilho, A. A. J. F. Castro, W. Castro, S. C. Ribeiro, F. Costa, R. C. De Oliveira, I. Coutinho, J. Cunha, L. Da Costa, L. Da Costa Ferreira, R. Da Costa Silva, M. Da Graça Zacarias Simbine, V. De Andrade Kamimura, H. C. De Lima, L. De Oliveira Melo, L. De Queiroz, J. R. De Sousa Lima, M. Do Espírito Santo, T. Domingues, N. C. Dos Santos Prestes, S. E. S. Carneiro, F. Elias, G. Eliseu, T. Emilio, C. L. Farrapo, L. Fernandes, G. Ferreira, J. Ferreira, L. Ferreira, S. Ferreira, M. F. Simon, M. A. Freitas, Q. S. García, A. G. Manzatto, P. Graça, F. Guilherme, E. Hase, N. Higuchi, M. Iguatemy, R. I. Barbosa, M. Jaramillo, C. Joly, J. Klipel, I. L. Do Amaral, C. Levis, A. S. Lima, M. L. Dan, A. Lopes, H. Madeiros, W. E. Magnusson, R. M. Dos Santos, B. Marimon, B. H. M. Junior, R. M. M. Grillo, L. Martinelli, S. M. Reis, S. Medeiros, M. Meira-Junior, T. Metzker, P. Morandi, N. M. Do Nascimento, M. Moura, S. C. Müller, L. Nagy, H. Nascimento, M. Nascimento, A. N. Lima, R. O. De Araújo, J. O. Silva, M. Pansonato, G. P. Sabino, K. M. P. De Abreu, P. J. F. P. Rodrigues, M. Piedade, D. Rodrigues, J. R. Rodrigues Pinto, C. Quesada, E. Ramos, R. Ramos, P. Rodrigues, T. R. De Sousa, R. Salomão, F. Santana, M. Scaranello, R. S. Bergamin, J. Schietti, J. Schöngart, G. Schwartz, N. Silva, M. Silveira, C. S. Seixas, M. Simbine, A. C. Souza, P. Souza, R. Souza, T. Sposito, E. S. Junior, J. D. Do Vale, I. C. G. Vieira, D. Villela, M. Vital, H. Xaud, K. Zanini, C. E. Zartman, N. K. H. Ideris, F. B. H. Metali, K. A. Salim, M. S. Saparudin, R. M. Serudin, R. S. Sukri, S. Begne, G. Chuyong, M. N. Djuikouo, C. Gonmadje, M. Simo-Droissart, B. Sonké, H. Taedoumg, L. Zemagho, S. Thomas, F. Baya, G. Saiz, J. S. Espejo, D. Chen, A. Hamilton, Y. Li, T. Luo, S. Niu, H. Xu, Z. Zhou, E. Álvarez-Dávila, J. C. A. Escobar, H. Arellano-Peña, J. C. Duarte, J. Calderón, L. M. C. Bravo, B. Cuadrado, H. Cuadros, A. Duque, L. F. Duque, S. M. Espinosa, R. Franke-Ante, H. García, A. Gómez, R. González-M., Á. Idárraga-Piedrahíta, E. Jimenez, R. Jurado, W. L. Oviedo, R. López-Camacho, O. A. M. Cruz, I. M. Polo, E. Paky, K. Pérez, A. Pijachi, C. Pizano, A. Prieto, L. Ramos, Z. R. Correa, J. Richardson, E. Rodríguez, G. M. Rodriguez M., A. Rudas, P. Stevenson, M. Chudomelová, M. Dancak, R. Hédl, S. Lhota, M. Svatek, J. Mukinzi, C. Ewango, T. Hart, E. K. Yakusu, J. Lisingo, J.-R. Makana, F. Mbayu, B. Toirambe, J. T. Mukendi, L. Kvist, G. Nebel, S. Báez, C. Céron, D. M. Griffith, J. E. G. Andino, D. Neill, W. Palacios, M. C. Peñuela-Mora, G. Rivas-Torres, G. Villa, S. Demissie, T. Gole, T. Gonfa, K. Ruokolainen, M. Baisie, F. Bénédet, W. Betian, V. Bezard, D. Bonal, J. Chave, V. Droissart, S. Gourlet-Fleury, A. Hladik, N. Labrière, P. Naisso, M. Réjou-Méchain, P. Sist, L. Blanc, B. Burban, G. Derroire, A. Dourdain, C. Stahl, N. N. Bengone, E. Chezeaux, F. E. Ondo, V. Medjibe, V. Mihindou, L. White, H. Culmsee, C. D. Rangel, V. Horna, F. Wittmann, S. Adu-Bredu, K. Affum-Baffoe, E. Foli, M. Balinga, A. Roopsind, J. Singh, R. Thomas, R. Zagt, I. K. Murthy, K. Kartawinata, E. Mirmanto, H. Priyadi, I. Samsoedin, T. Sunderland, I. Yassir, F. Rovero, B. Vinceti, B. Hérault, S.-I. Aiba, K. Kitayama, A. Daniels, D. Tuagben, J. T. Woods, M. Fitriadi, A. Karolus, K. L. Khoon, N. Majalap, C. Maycock, R. Nilus, S. Tan, A. Sitoe, I. Coronado G., L. Ojo, R. De Assis, A. D. Poulsen, D. Sheil, K. A. Pezo, H. B. Verde, V. C. Moscoso, J. C. C. Oroche, F. C. Valverde, M. C. Medina, N. D. Cardozo, J. De Rutte

Corzo, J. Del Aguila Pasquel, G. F. Llampazo, L. Freitas, D. G. Cabrera, R. G. Villacorta, K. G. Cabrera, D. G. Soria, L. G. Saboya, J. M. G. Rios, G. H. Pizango, E. H. Coronado, I. Huamantupa-Chuquimaco, W. H. Huasco, Y. T. H. Aedo, J. L. M. Peña, A. M. Mendoza, V. M. Rodriguez, P. N. Vargas, S. C. P. Ramos, N. P. Camacho, A. P. Cruz, F. R. Arevalo, J. R. Huaymacari, C. R. Rodriguez, M. A. R. Paredes, L. R. Bayona, R. Del Pilar Rojas Gonzales, M. E. R. Peña, N. S. Revilla, Y. C. S. Shareva, R. T. Trujillo, L. V. Gamarra, R. V. Martinez, J. V. Arenas, C. Amani, S. A. Ifo, Y. Bocko, P. Boundja, R. Ekoungoulou, M. Hockemba, D. Nzala, A. Fofanah, D. Taylor, G. Bañares-de Dios, L. Cayuela, Í. G. La Cerda, M. Macía, J. Stropp, M. Playfair, V. Wortel, T. Gardner, R. Muscarella, H. Priyadi, E. Rutishauser, K.-J. Chao, P. Munishi, O. Bánki, F. Bongers, R. Boot, G. Fredriksson, J. Reitsma, H. Ter Steege, T. Van Andel, P. Van De Meer, P. Van Der Hout, M. Van Nieuwstadt, B. Van Ulft, E. Veenendaal, R. Vernimmen, P. Zuidema, J. Zwerts, P. Akite, R. Bitariho, C. Chapman, E. Gerald, M. Leal, P. Mucunguzi, K. Abernethy, M. Alexiades, T. R. Baker, K. Banda, L. Banin, J. Barlow, A. Bennett, E. Berenguer, N. Berry, N. M. Bird, G. A. Blackburn, F. Brearley, R. Brienen, D. Burslem, L. Carvalho, P. Cho, F. Coelho, M. Collins, D. Coomes, A. Cuni-Sanchez, G. Dargie, K. Dexter, M. Disney, F. Draper, M. Duan, A. Esquivel-Muelbert, R. Ewers, B. Fadrique, S. Fauset, T. R. Feldpausch, F. França, D. Galbraith, M. Gilpin, E. Gloor, J. Grace, K. Hamer, D. Harris, K. Jeffery, T. Jucker, M. Kalamandeen, B. Klitgaard, A. Levesley, S. L. Lewis, J. Lindsell, G. Lopez-Gonzalez, J. Lovett, Y. Malhi, T. Marthews, E. McIntosh, K. Melgaço, W. Milliken, E. Mitchard, P. Moonlight, S. Moore, A. Morel, J. Peacock, K. S.-H. Peh, C. Pendry, R. T. Pennington, L. De Oliveira Pereira, C. Peres, O. L. Phillips, G. Pickavance, T. Pugh, L. Qie, T. Riutta, K. Roucoux, C. Ryan, T. Sarkinen, C. S. Valeria, D. Spracklen, S. Stas, M. Sullivan, M. Swaine, J. Talbot, J. Taplin, G. Van Der Heijden, L. Vedovato, S. Willcock, M. Williams, L. Alves, P. A. Loayza, G. Arellano, C. Asa, P. Ashton, G. Asner, T. Brncic, F. Brown, R. Burnham, C. Clark, J. Comiskey, G. Damasco, S. Davies, T. Di Fiore, T. Erwin, W. Farfan-Rios, J. Hall, D. Kenfack, T. Lovejoy, R. Martin, O. M. Montiel, J. Pipoly, N. Pitman, J. Poulsen, R. Primack, M. Silman, M. Steininger, V. Swamy, J. Terborgh, D. Thomas, P. Umunay, M. Uriarte, E. V. Torre, O. Wang, K. Young, G. A. Aymard C., L. Hernández, R. H. Fernández, H. Ramírez-Angulo, P. Salcedo, E. Sanoja, J. Serrano, A. Torres-Lezama, T. C. Le, T. T. Le, H. D. Tran, Taking the pulse of Earth's tropical forests using networks of highly distributed plots. *Biol. Conserv.* **260**, 108849 (2021).

19. Lopez-Gonzalez, G., Lewis, S.L., Burkitt, M., Phillips, O.L., ForestPlots. net: a web application and research tool to manage and analyse tropical forest plot data. *J. Veg. Sci.*, 610–613 (2011).

20. R. Condit, *Tropical Forest Census Plots* (Springer-Verlag Berlin Heidelberg New York Environmental Intelligence Unit, 1998).

21. R. Condit, R. Pérez, S. Aguilar, S. Lao, R. Foster, S. Hubbell, Complete data from the Barro Colorado 50-ha plot: 423617 trees, 35 years, version 3, Dryad (2019); https://doi.org/10.15146/5XCP-0D46.

22. J. K. Zimmerman, L. S. Comita, J. Thompson, M. Uriarte, N. Brokaw, Patch dynamics and community metastability of a subtropical forest: compound effects of natural disturbance and human land use. *Landsc. Ecol.* **25**, 1099–1111 (2010).

23. The Forest Inventory and Analysis Database: database description and user guide version 9.1 for Phase 2. U.S. Department of Agriculture, Forest Service. 1066 p. [Online]; https://www.fia.fs.usda.gov/library/database-documentation/index.

24. Forest Analysis and Inventory Branch, "Forest Inventory Ground Plot Data and InteracQve Map" (2023); heps://catalogue.data.gov.bc.ca/dataset/824e684b-4114-4a05-a490-aa56332b57f4.

25. Ministry of Forests, Wildlife and Parks, Networks of permanent sample plots in southern Quebec. Government of Quebec, Ministry of Forests, Wildlife and Parks, Forest Inventories Directorate, (2014); https://mffp.gouv.qc.ca/documents/forets/inventaire/Reseaux-PEP.pdf.

26. M. R. Easterling, S. P. Ellner, P. M. Dixon, SIZE-SPECIFIC SENSITIVITY: APPLYING A NEW STRUCTURED POPULATION MODEL. *Ecology* **81**, 694–708 (2000).

27. P. A. Zuidema, E. Jongejans, P. D. Chien, H. J. During, F. Schieving, Integral Projection Models for trees: a new parameterization method and a validation of model output. *J. Ecol.* **98**, 345–355 (2010).

28. G. Kunstler, A. Guyennon, S. Ratcliffe, N. Rüger, P. Ruiz-Benito, D. Z. Childs, J. Dahlgren, A. Lehtonen, W. Thuiller, C. Wirth, M. A. Zavala, R. Salguero-Gomez, Demographic performance of European tree species at their hot and cold climatic edges. *J. Ecol.* **109**, 1041–1054 (2021).

29. S. Ellner, D. Z. Childs, M. Rees, *Data- Driven Modelling of Structured Populations* (Springer International Publishing, 2016).

30. G. Piovesan, F. Biondi, On tree longevity. *New Phytol.* **231**, 1318–1337 (2021).

31. N. Rüger, R. Condit, D. H. Dent, S. J. DeWalt, S. P. Hubbell, J. W. Lichstein, O. R. Lopez, C. Wirth, C. E. Farrior, Demographic trade-offs predict tropical forest dynamics. *Science* **368**, 165–168 (2020).

32. J. F. Needham, D. J. Johnson, K. J. Anderson-Teixeira, N. Bourg, S. Bunyavejchewin, N. Butt, M. Cao, D. Cárdenas, C. Chang-Yang, Y. Chen, G. Chuyong, H. S. Dattaraja, S. J. Davies, A. Duque, C. E. N. Ewango, E. S. Fernando, R. Fisher, C. D. Fletcher, R. Foster, Z. Hao, T. Hart, C. Hsieh, S. P. Hubbell, A. Itoh, D. Kenfack, C. D. Koven, A. J. Larson, J. A. Lutz, W. McShea, J. Makana, Y. Malhi, T. Marthews, M. Bt. Mohamad, M. D. Morecroft, N. Norden, G. Parker, A. Shringi, R. Sukumar, H. S. Suresh, I. Sun, S. Tan, D. W. Thomas, J. Thompson, M. Uriarte, R. Valencia, T. L. Yao, S. L. Yap, Z. Yuan, H. Yuehua, J. K. Zimmerman, D. Zuleta, S. M. McMahon, Demographic composition, not demographic diversity, predicts biomass and turnover across temperate and tropical forests. *Glob. Change Biol.* **28**, 2895–2909 (2022).

33. S. Kambach, R. Condit, S. Aguilar, H. Bruelheide, S. Bunyavejchewin, C. Chang-Yang, Y. Chen, G. Chuyong, S. J. Davies, S. Ediriweera, C. E. N. Ewango, E. S. Fernando, N. Gunatilleke, S. Gunatilleke, S. P. Hubbell, A. Itoh, D. Kenfack, S. Kiratiprayoon, Y. Lin, J. Makana, M. Bt. Mohamad, N. Pongpattananurak, R. Pérez, L. J. V. Rodriguez, I. Sun, S. Tan, D. Thomas, J. Thompson, M. Uriarte, R. Valencia, C. Wirth, S. J. Wright,

S. Wu, T. Yamakura, T. L. Yao, J. Zimmerman, N. Rüger, Consistency of demographic trade-offs across 13 (sub)tropical forests. *J. Ecol.* **110**, 1485–1496 (2022).

34. N. Rüger, L. S. Comita, R. Condit, D. Purves, B. Rosenbaum, M. D. Visser, S. J. Wright, C. Wirth, Beyond the fast–slow continuum: demographic dimensions structuring a tropical tree community. *Ecol. Lett.* **21**, 1075–1084 (2018).

35. A. Esquivel-Muelbert, O. L. Phillips, R. J. W. Brienen, S. Fauset, M. J. P. Sullivan, T. R. Baker, K.-J. Chao, T. R. Feldpausch, E. Gloor, N. Higuchi, J. Houwing-Duistermaat, J. Lloyd, H. Liu, Y. Malhi, B. Marimon, B. H. Marimon Junior, A. Monteagudo-Mendoza, L. Poorter, M. Silveira, E. V. Torre, E. A. Dávila, J. Del Aguila Pasquel, E. Almeida, P. A. Loayza, A. Andrade, L. E. O. C. Aragão, A. Araujo-Murakami, E. Arets, L. Arroyo, G. A. Aymard C., M. Baisie, C. Baraloto, P. B. Camargo, J. Barroso, L. Blanc, D. Bonal, F. Bongers, R. Boot, F. Brown, B. Burban, J. L. Camargo, W. Castro, V. C. Moscoso, J. Chave, J. Comiskey, F. C. Valverde, A. L. Da Costa, N. D. Cardozo, A. Di Fiore, A. Dourdain, T. Erwin, G. F. Llampazo, I. C. G. Vieira, R. Herrera, E. Honorio Coronado, I. Huamantupa-Chuquimaco, E. Jimenez-Rojas, T. Killeen, S. Laurance, W. Laurance, A. Levesley, S. L. Lewis, K. L. L. M. Ladvocat, G. Lopez-Gonzalez, T. Lovejoy, P. Meir, C. Mendoza, P. Morandi, D. Neill, A. J. Nogueira Lima, P. N. Vargas, E. A. De Oliveira, N. P. Camacho, G. Pardo, J. Peacock, M. Peña-Claros, M. C. Peñuela-Mora, G. Pickavance, J. Pipoly, N. Pitman, A. Prieto, T. A. M. Pugh, C. Quesada, H. Ramirez-Angulo, S. M. De Almeida Reis, M. Rejou-Machain, Z. R. Correa, L. R. Bayona, A. Rudas, R. Salomão, J. Serrano, J. S. Espejo, N. Silva, J. Singh, C. Stahl, J. Stropp, V. Swamy, J. Talbot, H. Ter Steege, J. Terborgh, R. Thomas, M. Toledo, A. Torres-Lezama, L. V. Gamarra, G. Van Der Heijden, P. Van Der Meer, P. Van Der Hout, R. V. Martinez, S. A. Vieira, J. V. Cayo, V. Vos, R. Zagt, P. Zuidema, D. Galbraith, Tree mode of death and mortality risk factors across Amazon forests. *Nat. Commun.* **11**, 5515 (2020).

36. S. J. Wright, K. Kitajima, N. J. B. Kraft, P. B. Reich, I. J. Wright, D. E. Bunker, R. Condit, J. W. Dalling, S. J. Davies, S. Díaz, B. M. J. Engelbrecht, K. E. Harms, S. P. Hubbell, C. O. Marks, M. C. Ruiz-Jaen, C. M. Salvador, A. E. Zanne, Functional traits and the growth–mortality trade-off in tropical trees. *Ecology* **91**, 3664–3674 (2010).

37. L. Poorter, S. J. Wright, H. Paz, D. D. Ackerly, R. Condit, G. Ibarra-Manríquez, K. E. Harms, J. C. Licona, M. Martínez-Ramos, S. J. Mazer, H. C. Muller-Landau, M. Peña-Claros, C. O. Webb, I. J. Wright, ARE FUNCTIONAL TRAITS GOOD PREDICTORS OF DEMOGRAPHIC RATES? EVIDENCE FROM FIVE NEOTROPICAL FORESTS. *Ecology* **89**, 1908–1920 (2008).

38. D. M. A. Rozendaal, R. J. W. Brienen, C. C. Soliz-Gamboa, P. A. Zuidema, Tropical tree rings reveal preferential survival of fast-growing juveniles and increased juvenile growth rates over time. *New Phytol.* **185**, 759–769 (2010).

39. J. D. Hadfield, MCMC Methods for Multi-Response Generalized Linear Mixed Models: The **MCMCglmm** *R* Package. *J. Stat. Softw.* **33** (2010).

40. J. D. Hadfield, S. Nakagawa, General quantitative genetic methods for comparative biology: phylogenies, taxonomies and multi-trait models for continuous and categorical characters. *J. Evol. Biol.* **23**, 494–508 (2010).

41. F. Coelho De Souza, K. G. Dexter, O. L. Phillips, R. J. W. Brienen, J. Chave, D. R. Galbraith, G. Lopez Gonzalez, A. Monteagudo Mendoza, R. T. Pennington, L. Poorter, M. Alexiades, E. Álvarez-Dávila, A. Andrade, L. E. O. C. Aragão, A. Araujo-Murakami, E. J. M. M. Arets, G. A. Aymard C, C. Baraloto, J. G. Barroso, D. Bonal, R. G. A. Boot, J. L. C. Camargo, J. A. Comiskey, F. C. Valverde, P. B. De Camargo, A. Di Fiore, F. Elias, T. L. Erwin, T. R. Feldpausch, L. Ferreira, N. M. Fyllas, E. Gloor, B. Herault, R. Herrera, N. Higuchi, E. N. Honorio Coronado, T. J. Killeen, W. F. Laurance, S. Laurance, J. Lloyd, T. E. Lovejoy, Y. Malhi, L. Maracahipes, B. S. Marimon, B. H. Marimon-Junior, C. Mendoza, P. Morandi, D. A. Neill, P. N. Vargas, E. A. Oliveira, E. Lenza, W. A. Palacios, M. C. Peñuela-Mora, J. J. Pipoly, N. C. A. Pitman, A. Prieto, C. A. Quesada, H. Ramirez-Angulo, A. Rudas, K. Ruokolainen, R. P. Salomão, M. Silveira, J. Stropp, H. Ter Steege, R. Thomas-Caesar, P. Van Der Hout, G. M. F. Van Der Heijden, P. J. Van Der Meer, R. V. Vasquez, S. A. Vieira, E. Vilanova, V. A. Vos, O. Wang, K. R. Young, R. J. Zagt, T. R. Baker, Evolutionary heritage influences Amazon tree ecology. *Proc. R. Soc. B Biol. Sci.* **283**, 20161587 (2016).

42. B. Halliwell, L. A. Yates, B. R. Holland, "Multi-Response Phylogenetic Mixed Models: Concepts and Application" (preprint, Evolutionary Biology, 2022); https://doi.org/10.1101/2022.12.13.520338.

43. S. Díaz, J. Kattge, J. H. C. Cornelissen, I. J. Wright, S. Lavorel, S. Dray, B. Reu, M. Kleyer, C. Wirth, I. Colin Prentice, E. Garnier, G. Bönisch, M. Westoby, H. Poorter, P. B. Reich, A. T. Moles, J. Dickie, A. N. Gillison, A. E. Zanne, J. Chave, S. Joseph Wright, S. N. Sheremet'ev, H. Jactel, C. Baraloto, B. Cerabolini, S. Pierce, B. Shipley, D. Kirkup, F. Casanoves, J. S. Joswig, A. Günther, V. Falczuk, N. Rüger, M. D. Mahecha, L. D. Gorné, The global spectrum of plant form and function. *Nature* **529**, 167–171 (2016).

44. J. S. Joswig, C. Wirth, M. C. Schuman, J. Kattge, B. Reu, I. J. Wright, S. D. Sippel, N. Rüger, R. Richter, M. E. Schaepman, P. M. Van Bodegom, J. H. C. Cornelissen, S. Díaz, W. N. Hattingh, K. Kramer, F. Lens, Ü. Niinemets, P. B. Reich, M. Reichstein, C. Römermann, F. Schrodt, M. Anand, M. Bahn, C. Byun, G. Campetella, B. E. L. Cerabolini, J. M. Craine, A. Gonzalez-Melo, A. G. Gutiérrez, T. He, P. Higuchi, H. Jactel, N. J. B. Kraft, V. Minden, V. Onipchenko, J. Peñuelas, V. D. Pillar, Ê. Sosinski, N. A. Soudzilovskaia, E. Weiher, M. D. Mahecha, Climatic and soil factors explain the two-dimensional spectrum of global plant trait variation. *Nat. Ecol. Evol.* **6**, 36–50 (2021).

45. D. S. Maynard, L. Bialic-Murphy, C. M. Zohner, C. Averill, J. Van Den Hoogen, H. Ma, L. Mo, G. R. Smith, A. T. R. Acosta, I. Aubin, E. Berenguer, C. C. F. Boonman, J. A. Catford, B. E. L. Cerabolini, A. S. Dias, A. González-Melo, P. Hietz, C. H. Lusk, A. S. Mori, Ü. Niinemets, V. D. Pillar, B. X. Pinho, J. A. Rosell, F. M. Schurr, S. N. Sheremetev, A. C. Da Silva, Ê. Sosinski, P. M. Van Bodegom, E. Weiher, G. Bönisch, J. Kattge, T. W. Crowther, Global relationships in tree functional traits. *Nat. Commun.* **13**, 3185 (2022).

46. N. Carvalhais, M. Forkel, M. Khomik, J. Bellarby, M. Jung, M. Migliavacca, M. Mu, S. Saatchi, M. Santoro, M. Thurner, U. Weber, B. Ahrens, C. Beer, A. Cescatti, J. T. Randerson, M. Reichstein, Global covariation of carbon turnover times with climate in terrestrial ecosystems. *Nature* **514**, 213–217 (2014).

47. W. K. Cornwell, D. W. Schwilk, D. D. Ackerly, A TRAIT-BASED TEST FOR HABITAT FILTERING: CONVEX HULL VOLUME. *Ecology* **87**, 1465–1471 (2006).

48. S. E. Fick, R. J. Hijmans, WorldClim 2: new 1-km spatial resolution climate surfaces for global land areas. *Int. J. Climatol.* **37**, 4302–4315 (2017).

49. David Tilman, *Resource Competition and Community Structure. Princeton University Press, 1982.* (Princeton University Press, 1982).

50. D. Tilman, J. Knops, D. Wedin, P. Reich, M. Ritchie, E. Siemann, The Influence of Functional Diversity and Composition on Ecosystem Processes. *Science* **277**, 1300–1302 (1997).

51. J. Liang, T. W. Crowther, N. Picard, S. Wiser, M. Zhou, G. Alberti, E.-D. Schulze, A. D. McGuire, F. Bozzato, H. Pretzsch, S. de-Miguel, A. Paquette, B. Hérault, M. Scherer-Lorenzen, C. B. Barrett, H. B. Glick, G. M. Hengeveld, G.-J. Nabuurs, S. Pfautsch, H. Viana, A. C. Vibrans, C. Ammer, P. Schall, D. Verbyla, N. Tchebakova, M. Fischer, J. V. Watson, H. Y. H. Chen, X. Lei, M.-J. Schelhaas, H. Lu, D. Gianelle, E. I. Parfenova, C. Salas, E. Lee, B. Lee, H. S. Kim, H. Bruelheide, D. A. Coomes, D. Piotto, T. Sunderland, B. Schmid, S. Gourlet-Fleury, B. Sonké, R. Tavani, J. Zhu, S. Brandl, J. Vayreda, F. Kitahara, E. B. Searle, V. J. Neldner, M. R. Ngugi, C. Baraloto, L. Frizzera, R. Bałazy, J. Oleksyn, T. Zawiła-Niedźwiecki, O. Bouriaud, F. Bussotti, L. Finér, B. Jaroszewicz, T. Jucker, F. Valladares, A. M. Jagodzinski, P. L. Peri, C. Gonmadje, W. Marthy, T. O'Brien, E. H. Martin, A. R. Marshall, F. Rovero, R. Bitariho, P. A. Niklaus, P. Alvarez-Loayza, N. Chamuya, R. Valencia, F. Mortier, V. Wortel, N. L. Engone-Obiang, L. V. Ferreira, D. E. Odeke, R. M. Vasquez, S. L. Lewis, P. B. Reich, Positive biodiversity-productivity relationship predominant in global forests. *Science* **354**, aaf8957 (2016).

52. M. Sobral, M. Schleuning, A. Martínez Cortizas, Trait diversity shapes the carbon cycle. *Trends Ecol. Evol.*, S0169534723000617 (2023).

53. E. E. Butler, A. Datta, H. Flores-Moreno, M. Chen, K. R. Wythers, F. Fazayeli, A. Banerjee, O. K. Atkin, J. Kattge, B. Amiaud, B. Blonder, G. Boenisch, B. Bond-Lamberty, K. A. Brown, C. Byun, G. Campetella, B. E. L. Cerabolini, J. H. C. Cornelissen, J. M. Craine, D. Craven, F. T. de Vries, S. Díaz, T. F. Domingues, E. Forey, A. González-Melo, N. Gross, W. Han, W. N. Hattingh, T. Hickler, S. Jansen, K. Kramer, N. J. B. Kraft, H. Kurokawa, D. C. Laughlin, P. Meir, V. Minden, Ü. Niinemets, Y. Onoda, J. Peñuelas, Q. Read, L. Sack, B. Schamp, N. A. Soudzilovskaia, M. J. Spasojevic, E. Sosinski, P. E. Thornton, F. Valladares, P. M. van Bodegom, M. Williams, C. Wirth, P. B. Reich, Mapping local and global variability in plant trait distributions. *Proc. Natl. Acad. Sci.* **114** (2017).

54. H. Hillebrand, On the Generality of the Latitudinal Diversity Gradient. *Am. Nat.* **163**, 192–211 (2004).

55. T. I. Kohyama, D. Sheil, I.-F. Sun, K. Niiyama, E. Suzuki, T. Hiura, N. Nishimura, K. Hoshizaki, S.-H. Wu, W.-C. Chao, Z. S. Nur Hajar, J. S. Rahajoe, T. S. Kohyama, Contribution of tree community structure to forest productivity across a thermal gradient in eastern Asia. *Nat. Commun.* **14**, 1113 (2023).

56. Lalasia Bialic-Muphphy, Robert McElderry, The pace of life for forest trees, Zenodo (2024); https://doi.org/10.5281/zenodo.11615767.

57. POWO (2024). "Plants of the World Online. Facilitated by the Royal Botanic Gardens, Kew. Published on the Internet; http://www.plantsoftheworldonline.org/ Retrieved 17 June 2024."

58. F. Specker, A. Paz, T. W. Crowther, D. S. Maynard, Treemendous: an R package for integrating taxonomic information across backbones. *PeerJ* **12**, e16896 (2024).

59. R Core Team, R: A language and environment for statistical computing, (2022); https://www.R-project.org/.

60. S. Muff, E. B. Nilsen, R. B. O'Hara, C. R. Nater, Rewriting results sections in the language of evidence. *Trends Ecol. Evol.* **37**, 203–210 (2022).

61. D. Bates, M. Mächler, B. Bolker, S. Walker, Fitting Linear Mixed-Effects Models Using **lme4**. *J. Stat. Softw.* **67** (2015).

62. J. Needham, C. Merow, C.-H. Chang-Yang, H. Caswell, S. M. McMahon, Inferring forest fate from demographic data: from vital rates to population dynamic models. *Proc. R. Soc. B Biol. Sci.* **285**, 20172050 (2018).

63. M. Maechler, Rousseeuw P., Struyf A., Hubert M., Hornik K., cluster: Cluster Analysis Basics and Extensions, (2022).

64. L. Poggio, L. M. de Sousa, N. H. Batjes, G. B. M. Heuvelink, B. Kempen, E. Ribeiro, D. Rossiter, SoilGrids 2.0: producing soil information for the globe with quantified spatial uncertainty. *SOIL* **7**, 217–240 (2021).

65. H. Qian, Y. Jin, An updated megaphylogeny of plants, a tool for generating plant phylogenies and an analysis of phylogenetic community structure. *J. Plant Ecol.* **9**, 233–239 (2016).

66. Y. Jin, H. Qian, V.PhyloMaker2: An updated and enlarged R package that can generate very large phylogenies for vascular plants. *Plant Divers.* **44**, 335–339 (2022).

67. D. Cardoso, R. T. Pennington, L. P. De Queiroz, J. S. Boatwright, B.-E. Van Wyk, M. F. Wojciechowski, M. Lavin, Reconstructing the deep-branching relationships of the papilionoid legumes. *South Afr. J. Bot.* **89**, 58–75 (2013).

68. D. N. Karger, O. Conrad, J. Böhner, T. Kawohl, H. Kreft, R. W. Soria-Auza, N. E. Zimmermann, H. P. Linder, M. Kessler, Climatologies at high resolution for the earth's land surface areas. *Sci. Data* **4**, 170122 (2017).

Acknowledgments: We warmly thank the international team of network collaborators, including those who are not co-authors on this paper, for sharing their valuable plot datasets and providing their insights and support for this project. This study was enabled by the Global Forest Dynamics database, initiated by the TreeMort project, on which this study is based. The tropical tree analyses were enabled by the Forestots.net research project #169 ('Placing life history trait variation of forest trees in an evolutionary and environmental context'). ForestPlots.net is a global collaboration and meta-network supported from the

University of Leeds(*18*, *19*). **Funding:** TP, AEM, and OLP acknowledge support from the European Research Council (ERC) under the European Union's Horizon 2020 research and innovation programme (grant agreement 758873, TreeMort). AE-M was further funded by the Royal Society Standard Grant RGS\R1\221115 'MegaFlora', the UKRI/NERC TreeScapes NE/V021346/1 'MEMBRA', the NERC/NSF Gigante NE/Y003942/1 and the FRB/CESAB 'Syntreesys'. OLP and ForestPlots.net data management have been supported by several grants including from the UK Natural Environment Research Council ('AMSINK' NE/X014347/1, 'SECO' NE/T012722/1, 'BIO-RED' NE/N012542/1, 'ARBOLES' NE/S011811/1) as well as from the European Research Council, the European Space Agency, the European Union and the Royal Society. ForestPlots.net partners acknowledge many additional sources of funding: Instituto Nacional de Ciência e Tecnologia (INCT) grant ID #465610/2014-5], FAPEG grant ID #201810267000023, CNPq (PELD CNPq 403710/2012-0, and CNPq/Universal grant 459941/2014-3), British Natural Environment Research Council/NERC (NE/K016431/1), FAPESP (BIOTA grants 2003/12595-7; 2012/51509-8 and 2012/51872-5); doctoral and postdoctoral fellowships from (FAPESP 11/11604-0 and 22/09041-0), as well as Project Sustainable Landscapes (US Forest Service, USAID, EMBRAPA & NASA-Goddard), National Council for Scientific and Technological Development (CNPq), PELD-TRAN 441244/2016-5 and 441572/2020-0, Mato Grosso State Research Support Foundation (FAPEMAT) – 0346321/202, the NERC Knowledge Exchange Fellowship (grant ref no. NE/V018760/1), NERC Amazon Past Fire Project NE/N011570/1, CAPES Project PVE177-2012, CNPq grants 441282/2016-4, 403764/2012-2 and 558244/2009-2 for IAFA LTER plots, FAPEAM grants 1600/2006, 465/2010 and PPFOR 147/2015, CNPq grants 473308/2009-6 and 558320/2009-0 funded the monitoring of Purus-Madeira interfluve. The BCI forest dynamics research project was made possible by National Science Foundation grants to Stephen P. Hubbell: DEB-0640386, DEB-0425651, DEB-0346488, DEB-0129874, DEB-00753102, DEB-9909347, DEB-9615226, DEB-9615226, DEB-9405933, DEB-9221033, DEB-9100058, DEB-8906869, DEB-8605042, DEB-8206992, DEB-7922197, support from the Forest Global Earth Observatory (ForestGEO), the Smithsonian Tropical Research Institute, the John D. and Catherine T. MacArthur Foundation, the Mellon Foundation, the Small World Institute Fund, and numerous private individuals, and through the hard work of over 100 people from 10 countries over the past three decades. Research at the Wabikon Forest Dynamics Plot was supported by the 1923 Fund and the Cofrin Center for Biodiversity at the University of Wisconsin-Green Bay and the U.S. Forest Service. The Luquillo ForestGeo dataset was supported by grants BSR-8811902, DEB 9411973, DEB 0080538, DEB 0218039, DEB 0620910, DEB 0963447 AND DEB-129764 from NSF to the Department of Environmental Science, University of Puerto Rico, and to the International Institute of Tropical Forestry, USDA Forest Service, as part of the Luquillo Long-Term Ecological Research Program. The U.S. Forest Service (Dept. of Agriculture) and the University of Puerto Rico gave additional support. The BIC, Luquillo, and Wabikon plots were part of the Smithsonian Institution Forest Global Earth Observatory, a worldwide network of large, long-term forest dynamics plots. TP and JA acknowledge funding from the CLIMB-FOREST Horizon Europe Project (No 101059888) that was funded by the European Union. GD acknowledges support from an "Investissement d'Avenir" grant managed by Agence Nationale de la Recherche (CEBA, ref. ANR-10-LABX-25-01*)*. **Author contributions:** LBM led the writing of this manuscript, with substantial input from T.W.C., R.M.M., A.E.M., J.v.d.H, P.A.Z. and T.P. LBM led the analysis, with input from R.M.M and P.A.Z. AEM, TP, OP, JA, KMB, and LMB assembled and integrated the tree dynamics database, with contributions from other ForestPlots and TreeMort network partners. All authors collected and curated data from inventory plots, provided feedback on the results, and contributed to the writing of the manuscript.

Competing interest: The authors have no competing interests. **Data availability statement:** The plot-level input data and R code that are needed to replicate our analyses are available at https://github/Lalasia/pace_of_life.com and doi.org/10.5281/zenodo.11615767 (*56*). The tree-by-tree observations used to generate the plot-level input data are also published with this paper. However, this file does not include data from networks with sensitive species or a need for indigenous data sovereignty. These data are available upon request for research purposes by emailing the following networks: Alberta Agriculture and Forestry Division https://www.alberta.ca/permanent-sample-plots-program, email: af.fmb-biometrics@gov.ab.ca, Saskatchewan Minister of Environment Forest Service Branch https://www.saskatchewan.ca/contact-us, ForestGeo https://forestgeo.si.edu/explore-data ((*20–22*), and ForestPlots https://forestplots.net/en/using-forestplots/in-the-field, email: admin@forestplots.net (*18*, *19*).

Supplementary Materials:
Materials and Methods
Figs. S1 to S15
Tables S1 to S7
References (54-68)

Supplementary Materials for
The pace of life for forest trees

Lalasia Bialic-Murphy[1], Robert M. McElderry[1,2], Adriane Esquivel-Muelbert[3], Johan van den Hoogen[1], Pieter A. Zuidema[4], Oliver Phillips[5], Edmar Almeida de Oliveira[6], Patricia Alvarez Loayza[7], Esteban Alvarez-Davila[8], Luciana F. Alves[9], Vinícius Andrade Maia[10], Simone Aparecida Vieira[11], Lidiany Carolina Arantes da Silva[10], Alejandro Araujo-Murakami[12], Eric Arets[13], Julen Astigarraga[14], Fabrício Baccaro[15], Timothy Baker[5], Olaf Banki[16], Jorcely Barroso[17], Lilian Blanc[18], Damien Bonal[19], Frans Bongers[20], Kauane Maiara Bordin[21], Roel Brienen[5], Marcelo Brilhante de Medeiros[22], José Luís Camargo[23], Felipe Carvalho Araújo [10], Carolina V. Castilho[24], Wendeson Castro[25], Victor Chama Moscoso[26], James Comiskey[27,28], Flívia Costa[29], Sandra Cristina Müller [21], Everton Cristo de Almeida[30], Lola da Costa[31], Vitor de Andrade Kamimura[32], Fernanda de Oliveira[10], Jhon del Aguila Pasquel[33,34], Géraldine Derroire[35], Kyle Dexter[36], Anthony Di Fiore[37,38], Louis Duchesne[39], Thaise Emílio [40], Camila Laís Farrapo[10], Sophie Fauset[41], Federick C. Draper[42], Ted R. Feldpausch[43], Rafael Flora Ramos[44], Valeria Forni Martins[45,21], Marcelo Fragomeni Simon[46], Miguel Gama Reis[10], Angelo Gilberto Manzatto[47], Bruno Herault[48,18], Rafael Herrera[49], Eurídice Honorio Coronado[50], Robert Howe[51], Isau Huamantupa-Chuquimaco[52], Walter Huaraca Huasco[53], Katia Janaina Zanini[21], Carlos Joly[54], Timothy Killeen[55], Joice Klipel[21], Susan G. Laurance[56], William F. Laurance[56], Marco Aurélio Leite Fontes[10], Wilmar Lopez Oviedo[57], William E. Magnusson[58], Rubens Manoel dos Santos[10], Jose Luis Marcelo Peña [59], Karla Maria Pedra de Abreu[60], Beatriz Marimon[61], Ben Hur Marimon Junior[6], Karina Melgaço [62], Omar Aurelio Melo Cruz[63], Casimiro Mendoza[64], Abel Monteagudo-Mendoza[65], Paulo S. Morandi[6], Fernanda Moreira Gianasi[10], Henrique Nascimento[66], Marcelo Nascimento[67], David Neill[68], Walter Palacios[69], Nadir C. Pallqui Camacho[5], Guido Pardo[70], R. Toby Pennington[71,72], Maria Cristina Peñuela-Mora[73], Nigel C.A. Pitman[74], Lourens Poorter[4], Adriana Prieto Cruz[75], Hirma Ramírez-Angulo[76], Simone Matias Reis[77,6], Zorayda Restrepo Correa[78], Carlos Reynel Rodriguez[79], Agustín Rudas Lleras[80], Flavio A. M. Santos[54], Rodrigo Scarton Bergamin[81], Juliana Schietti[15], Gustavo Schwartz[82], Julio Serrano[83], André Maciel Silva-Sene[10], Marcos Silveira[84], Juliana Stropp[85], Hans ter Steege[16], John Terborgh[86], Mathias W. Tobler[87], Luis Valenzuela Gamarra[55], Peter J. van de Meer[88], Geertje van der Heijden[89], Rodolfo Vasquez[90], Emilio Vilanova[91], Vincent Antoine Vos[92], Amy Wolf[93], Christopher W. Woodall[94], Verginia Wortel[95], Joeri A. Zwerts[96], Thomas A.M. Pugh[97,3], Thomas W. Crowther[1]

***Corresponding author e-mail:** lalasia.bialicmurphy@usys.ethz.ch

The PDF file includes:

Materials and Methods
Figs. S1 to S15
Tables S1 to S7
References (57-68)

Materials and methods

1: Forest inventory data

The dataset we used for this project was developed by a global community of network partners, including members of the ForestPlots (*18*), TreeMort, and ForestGeo networks (*20–22*), and includes dynamic tree data from thousands of long-term research plots and datasets from National Forest Inventory networks (table S1). Combining and quality controlling this network of dynamic tree data was led by the Global Forest Dynamics team, initiated by the TreeMort project, and the ForestPlots network (*18*). The compiled dataset includes the following information: tree ID, diameter at breast height (dbh) at 1.3 m of trunk height, status (alive or dead), plot ID, plot coordinates, census year, and management history. Tree species names were standardized across the datasets using The World Consensus on Vascular Plants backbone (*57*) and the `Treemendous` R package (*58*). The point of dbh measurement differed by > 30 cm in a few cases for predominantly tropical trees, in which case we excluded the census points. To standardize our life history trait comparisons among species, we excluded tree observation < 10 cm dbh. The time interval between census periods varied from 1 to 36 years, with the highest occurrence of a 5-year census interval. Since time intervals greater than 10 years were not represented across all datasets and were sparse overall, we excluded census intervals >10 years. Thus, we focused on interval lengths that were well-represented across the forest inventory datasets. The plot size ranged from 0.07 ha to 50 ha among forest inventories. Tree observations with 'unnatural' modes of death (i.e., harvest, etc.) were removed from our analysis because they do not reflect 'ambient' life history dynamics. We limited our analysis to species with >100 unique observations and excluded species with < 5 observed deaths to maintain a sufficient sample size and excluded tree observations with unknown species identity. We also exclude species that did not have observations across species size ranges (i.e., there were only observations for large-sized individuals, with no information for smaller individuals in the 10 cm dbh size range). To balance our dataset across our biogeographic gradient, we randomly sub-sampled the North American plots to equal the number of point observations in Central and South America (see materials and methods). This allowed us to avoid potential biases due to imbalanced sampling efforts across our biogeographic gradients. These initial filters reduced the dataset from 5.6 million unique observations of 5,612 species to 3.2 million unique tree measurements for 1,127 species (i.e., tree size and status) (Table S1).

All analyses were conducted in R version 4.2.0 (*59*). While p-values and R^2 are reported for generalized linear models, we present results in terms of 'evidence' versus significance levels, following (*60*).

2: Integral projection models

2.1 Assigning individual tree observations to hexagon grid IDs

To capture the full range of life history strategies across a latitudinal gradient, we used Google Earth Engine to assign each tree measurement (dbh and status) to equal area hexagon grids (size ~ 250,000 km^2) (fig S1). The hexagon grid ID was then included as a categorical random effect in our species-specific survival and growth models. This allowed us to incorporate intra-specific variation in tree life history traits (growth strategies, stature, and longevity) across broadscale biogeographic gradients (see material and methods, subsection 2.2-2.5). The unique hexagon grid IDwere also used to calculate the demographic trait diversity (convex-hull volume in life history trait space that is occupied by species within each grid) and characterize the relationship between demographic trait diversity and above-ground net primary productivity (see material and methods, subsection 4).

2.2 Species-specific survival and growth models

To estimate size-dependent survival and growth rate coefficients for our integral projection models (IPM), we fit species-specific generalized linear mixed-effect models, using the `glmer` and the `lmer` function in the `lme4` package (*61*). Here y_{ij} is the response for individual i in grid cell j. The random grid cell effect, μ_j, and error, ϵ_{ij}, are added to the intercept, b0. The effect of size, x_{ij}, for individual i in grid cell j is measured by the slope, b1. Our survival model included 'initial tree size' (dbh) and the square of tree size (centered natural log of dbh) as predictor variables, survival at the second census interval as the response variable, and grid ID as a random effect. Similarly, for our growth model, we included initial tree size (dbh) as a predictor variable, size at the second census interval as the response variable, and grid ID as a random effect. Tree size was natural log-transformed for both models.

$$y_{ij} = \beta_0 + \beta_1 x_{ij} + \mu_j + \epsilon_{ij}$$

To account for variation in forest inventory census intervals, we standardized the survival and growth rate estimates to a one-year time-step. This was relatively straightforward for survival but more involved for growth. Specifically, for our survival model, we fit a logistic regression with a complementary log-log link function and included the census interval length as an offset, which effectively standardized the survival rate to a 1-year timestep. To standardize the time step for our growth model, we tested two approaches. First, we calculated the relative growth rate (RGR), which is the geometric mean of the ratio of log tree sizes over the time interval, $rgr = (s_t/s_0)^{1/t}$. Here, rgr is the annualized relative growth rate, s_0 is the log of the initial size, and s_t is the log of size at the end of the time interval, t. We calculated size in the next year for all initial tree observations by multiplying the initial size by the annualized growth rate, $s_1 = s_0 rgr$. This method implicitly assumes a zero intercept in the growth function. To test if the assumption of a zero intercept influenced our results, we explored a second method that directly computes the annual slope and intercept for a variable time interval. The algebraic expression that represents the compounding effect of adding an intercept in each annual estimate within a time series results in a nonlinear expression. Thus, we employed the nonlinear least squares function to estimate the following model, $s_t = \mathrm{b}_0(1 - \mathrm{b}_1{}^t)/(1 - \mathrm{b}_1) + s_0 \mathrm{b}_1{}^t)$. Visual inspection of coefficient plots and model fit plots using both methods showed highly similar results. Due to the extended computation time for the nonlinear models, we chose the less complex RGR method, and converted final size, s_t, to size at one year, s_0, before fitting our growth regressions.

Model evaluation of our vital rate regressions showed that initial tree size captured a high amount of variance for our growth models and was a significant predictor of tree size in the following timestep (R^2=0.83-0.99, and $p < 0.001$). Similarly, initial size was a significant predictor of survival ($p < 0.001$). It is important to note that, for nonlinear regression models, the R^2 does not represent the proportion of variance explained by the predictor variable and is thus not a useful metric for evaluating the goodness of fit for logistic regression. For this reason, we did not report this value for our survival models.

2.3 Size-dependent integral projection model

An integral projection model (IPM) is a tractable way to derive life history traits, using continuous size-based survival and growth rates. To calculate age-related traits from size-dependent probabilities, we used a key component of an IPM, the survival-growth kernel, **P**, and with methods developed by (*26*), we projected the future fate of living individuals. By

excluding reproduction, this model captures cohort dynamics based on survival and growth rates. A change in the size-specific density of trees, $n(t)$, is projected using the following equation:

$$n(y, t+1) = \int_{l}^{u} \mathbf{P}(\mathrm{y}, \mathrm{x}) n(x, t) dx$$

where the kernel $\mathbf{P}(\mathrm{y}, \mathrm{x})$ is a non-negative surface of survival and growth transition probabilities of individual plants from size *x* at time *t* to size *y* at time *t*+1. L and U represent the minimum and maximum plant size thresholds respectively, with the lower threshold L being set to 10 cm dbh and the upper size threshold being set to the species maximal tree size. **P** is composed of two functions,

$$\mathbf{P}(\mathrm{y}, \mathrm{x}) = \mathrm{s}(x)\mathrm{g}(\mathrm{y}, \mathrm{x})$$

where $\mathrm{s}(\mathrm{x})$ represents the survival rate of an *x*-sized individual and growth $\mathrm{g}(\mathrm{y}, \mathrm{x})$ is the probability density for individuals of size *x* transitioning to size *y* over a 1-year timestep. These parameters are derived from the species- and grid-cell-specific survival and growth regression models that we parameterized with empirical field data (see materials and methods, subsection 2.2).

Our species- and grid cell-specific IPMs were informed by hundreds to thousands of unique tree measurements across a large portion of a species life cycle (from 10 cm dbh to their maximal size) and across a wide range of local conditions (light and nutrient conditions, varying levels of density dependence, etc.). This framework allowed us to explicitly account for survival-growth trade-offs that operate across species life cycles and thus provide a tractable way to calculate robust species-level mean life history trait estimates (passage time and life expectancy) across broadscale biogeographic gradients (i.e., for each species by grid cell combination).

2.4 IPM kernel integration and diagnostic checks

The relatively slow incremental growth of trees can create a sharp ridge along the diagonal of the probability surface, **P**. Defining this ridge with sufficiently high resolution becomes computationally expensive when numerically integrating the kernel, **P**, and failing to do so can lead to biologically unreasonable column sums, which theoretically equal the survival rate for each size class. Previous work indicates that IPM model outputs for trees (first passage times, etc.) are sensitive to the dimension used for kernel integration, whereby a small kernel size (i.e., 10 size categories) can underestimate tree age demographics and a large kernel size (i.e., 1,000 size categories) can overestimate tree age demographics. Thus, previous works show that a kernel dimension equivalent to a tree size transition rate between 0.1-1 cm in diameter is needed to produce realistic tree age demographics for trees (*27*). Thus, to balance the need for high biological resolution and reduced computation time and memory, a mixed kernel integration approach has been established for trees (*27–29*). Following this mixed kernel integration approach, we selected a moderately large resolution for the overall kernel, 600 × 600, and used the standard mid-bin integration for most of these cells. Along the growth ridge, we used a Gaussian-Legendre quadrature integration, whereby each cell was divided into 420 sub-rows (i.e., along the size-dependent growth probability density) and 3 sub-columns. The result was a 600 × 600 kernel with a well-defined ridge and biologically reasonable column sums and element values.

2.5 Life history trait calculations and age-from-stage methods

Following numerical integration, the survival-growth kernel, **P**, was used to calculate a series of life history traits, including first passage time, life expectancy from 10 cm dbh, and maximal lifespan. These life history traits were derived from survival and growth data that were collected between 1926 and 2014. These life history traits are thus representative of tree age demographics based on observed climate conditions over the last century.

Passage time: First passage time captures the number of years it takes for an *x*-sized individual to reach a predetermined size threshold for the first time. Using the kernel, **P**, we calculated passage time τ_{ij} from initial size class *j* to the target size class *i*, following (*15–17*) :

$$\tau_{ij} = \frac{(\mathbf{I} - \mathbf{P}')^{-2}(i,j)}{(\mathbf{I} - \mathbf{P}')^{-1}(i,j)}$$

where **I** is an identity matrix and **P′** is identical to **P** except for column j, which is replaced with zeros in all cells. The initial size for all passage time calculations was 10 cm dbh because this is the size when all species were tagged in our standardized dataset. Throughout the main text, we refer to our passage time to target size thresholds as tree *growth strategies*.

To make biologically reasonable comparisons in growth strategies among species, we calculated first passage times to 20 cm dbh (fig. S2, path a.2) and the 70% quantile of observed maximal size (fig. S2, path a.1). The 20 cm target size threshold serves as a time-standardized rate of growth for all species in our dataset. However, the passage time from 10 to 20 cm dbh may represent the time to max size for the smallest statured species in our dataset (i.e., 20 cm size is the 95% quantile of maximum size for small trees). Conversely, this target threshold captures early life growth dynamics for larger tree species. To capture growth dynamics over a wider range of a species life cycle, we also calculated the first passage time from 10 cm DHB to the 70% quantile of the observed size distribution for each species across the full dataset. This quantile-based target size varied among species and represented an above-average size at which point a tree has approached its ultimate position in the canopy, whether that be a short-statured understory tree that reaches its maximal height in 5-years or a tall dominant canopy tree that grows for decades before reaching their ultimate position in the canopy.

Life expectancy: To examine differences in early-life tree mortality patterns and survivorship trajectories over species lifespans, we calculated life expectancy from size class *i* to size class *j* using (fig. S2, path b) (*1*, *15–17*):

$$\eta_j = \sum_{i=1}^{n} (\mathbf{I} - \mathbf{P})^{-1}(i,j)$$

where **I** is an identity matrix. Life expectancy from 10 cm dbh was calculated using the equation above with *j* = 1. For total life expectancy conditional on reaching the target size classes (either 20cm dbh or the 70th quantile of a species size distribution), we determined which column, j, corresponded to the target class and then added the time to reach size class *j* to the remaining life expectancy for size class *j*, i.e., $\tau_{ij} + \eta_i$. It is important to note that life expectancy is highly left skewed by early life mortality, with smaller individuals having higher mortality than larger individuals. A low life expectancy to a given size (e.g., 20 cm dbh) does not imply that no individuals of a given species will survive to that size threshold

(i.e., it is not a maximal). It simply means that individuals that do live longer represent the lucky few, resulting in a higher proportion of smaller individuals within a population.

Maximal lifespan: We calculated the maximal lifespan as the age at which the cumulative mortality was 95%. Starting with a cohort composed exclusively of 10 cm dbh individuals, we projected the cohort through time using the recursion equation $n(t+1) = \mathbf{P}n(t)$. The simulation limit was set to 10,000, which resulted in the exclusion of 38 species. We normalized the initial cohort to sum to one and identified the time step, *x*, where the sum of $n(x)$ was less than 0.05. The number of years, *x*, is thereby the age at which less than 5% of the initial cohort is still alive. At this maximal age, *x*, we also calculated the mean size from the population density, $n(x)$, which we refer to in the main text as *size at maximal age*.

Model valuation: We parameterized our IPMs using methods that were specifically developed for cross-sectional tree data (see materials and methods, subsection 2.4) (*27–29*) and used age-from-stage methods to calculate age-related demographics (*15–17*). Validation of age-related outputs would require an extensive longitudinal dataset that tracks the fate of individual trees over their life cycle (which would require decades to millennia of longitudinal data for long-lived trees). This level of longitudinal data is rarely available and is also why cross-sectional forest inventory data and age-from-stage estimates are so valuable. The next best validation method relies on tree ring data. Previous validations of IPM model outputs for trees with paired tree ring data showed that IPMs can produce realistic estimates of tree age demographics (*27*). Similarly, IPM model validations, using 34-year time series data, showed that IPM outputs match time series data over snapshots of species life cycles (*62*). Together, previous validation efforts for IPMs using time series and tree ring data suggest model outputs can accurately capture the age dynamics for long-lived species with slow growth and low mortality. We did not have such paired time series or tree ring data to compare with the wide range of species included in our analysis. Yet, while not directly comparable, the directionality of our biome-level comparisons in tree longevity was congruent with longevity estimates from tree ring data (*12*). Specifically, that assessment showed that the mean longevity for trees in the tropics and extratropics were 186 $\pm$138 and 322$\pm$ 201 years respectively (*12*). In our study, we found that the mean life expectancy for trees in the tropics and extratropics were 60 and 95 years respectively (see Figure 2).

While the directionality of our biome-level patterns in tree longevity is in line with broadscale trends derived from tree ring studies, there are several reasons why it does not make conceptual sense to make one-to-one comparisons in measures of tree longevity derived from IPMs from that of tree ring-studies that differ in temporal times scales and geographical scope. First, age estimates from tree-ring studies can be heavily influenced by anthropogenic disturbance and climate-induced shifts in tree growth-longevity trade-offs. Second, the sampling framework used for tree ring studies tends to target the largest trees in areas of low anthropogenic disturbance. Yet, considering that the oldest trees can be up to half the size of the largest trees (*30*), it is impossible to derive standardized metrics of tree age (e.g., mean life expectancy) from tree ring studies and thus they serve as a coarse estimate of tree longevity.

3: Tree life history trade-offs and core demographic functional types

To test for broadscale tree growth- longevity-stature trade-offs, we conducted a correlation analysis, using the `cor` function in the `stats` package (*59*). To further contextualize the full dimensionality of growth- longevity-stature trait constellations, we conducted a standard principal component analysis (PCA) of the life history traits, using the `princomp` function

in the `stats` package (*59*). All traits included in the PCA were scaled to have a mean of zero and a standard deviation of one. Highly correlated traits that captured redundant trait information were dropped from the PC analysis to avoid issues of multicollinearity, resulting in the inclusion of passage time to 20 cm dbh, passage time to 70th quantile size range, size at maximal age, and life expectancy from 10 cm dbh (fig. S3). We then used the K-means machine learning algorithm to identify the core growth- longevity- stature groupings, setting the maximum number of iterations to 15 and the number of random starting points to 50, using the `kmeans` function in the R `stats` package. To identify the optimal number of clusters, we calculated the coefficient scores and the total within sum of squares across cluster sizes, using the `silhouette` and `wss` functions in the R `cluster` package (*63*). The sum of squares elbow method (wss) and the silhouette method both indicated that 4 was the optimal number of clusters, and the silhouette method identified 3 as the second optimal number of clusters (fig. S5).

4: The strength of tree life history trade-offs across biogeographic gradients:
To examine the independent and joint effects of soil, precipitation, and temperature on tree life history traits we used a multivariate Bayesian generalized mixed effect model, using the `MCMCglmm` package in R (*39*). We included the same four life history traits used in S3 as response variables (i.e., time to 20cm, time to 70th percentile of size, size at maximal age, and life expectancy from 10cm dbh) and soil, precipitation, and temperature indexes as fixed effects (described below). To account for the signature of phylogenetic ancestry on tree life history traits, we included the phylogenetic distances between species as a random effect (*39*, *42*). We also controlled for the covariation between our life history traits and the residual variation within each trait response to account for potential trade-offs among life history traits (*39*). To meet model assumptions, we scaled our life history traits and climate variables to a mean of zero standard deviation of one.

<u>Biogeographic indexes:</u> We included soil, precipitation, and temperature indexes in our Bayesian model because they are known to strongly regulate photosynthetic capacity and plant growth and are commonly assumed to induce life history trade-offs. To avoid issues with multicollinearity and reduce model complexity, we first extracted a comprehensive set of variables related to soil, temperature, and precipitation from WorldClim and SoilGrids (*64*) and calculated the mean of these variables for each grid cell, using Google Earth Engine (see fig. S1 and table S4). We then assigned each variable to a categorical soil, climate, or precipitation grouping (table S4) and conducted a principal component analysis for the list of variables within each group. The first PC axis for each group (e.g., soil, precipitation, and temperature indexes) were then included as fixed effects in our Bayesian generalized mixed effect model. These soil, temperature, and precipitation indexes represent multi-year mean conditions from 1997-2013. These multi-year averages capture the mean conditions that correspond with the dynamical data used to calculate our age-related demographic traits (e.g., mean life expectancy of trees based on observation data from the 1900s-2000s).

<u>Phylogenetic tree:</u> We constructed the time-calibrated phylogeny for all tree species using the Qian and Jin 2016 megaphylogeny (*65*) for plants and the `V.Phylomaker2` (*66*) package in R. The three species that were missing from the phylogenetic backbone were added to the tree using the most closely related species within the same genus, following Cardoso et. Al 2013 (*67*).

<u>Bayesian model construction and validation:</u> The multivariate Bayesian models were run with 15,000 iterations, a burnin of 5,000, and a thinning rate of 10, with an effective sample size

of 1000 MCMC samples. Model convergence was assessed via inspection of trace and density plots. Posterior means and upper and lower credible intervals for the fixed and random effects were used to examine the shared influence of phylogenetic ancestry and soil, temperature, and precipitation variables on mean life history trait differences across our biogeographic gradient (figs. S9 and S11, table S5-S9). The estimated variance coefficients for the fixed and random effects are reported in figs. S9 and S11, Table S5-S9. Credible intervals that do not overlap with zero are suggestive of mean trait differences across broadscale soil, temperature, and precipitation gradients. The phenotypic variance-covariance, genetic variance-covariance and residual variance-covariance, and Pagels lambda (i.e., phylogenetic heritability) are reported in Table S6.

5: Demographic trait diversity across biogeographic gradients

To characterize the range of life history strategies that were occupied by species across broadscale biogeographic gradients, we first calculated the 3-dimentional convex-hull volume of tree growth-longevity-stature strategies (i.e., demographic trait diversity) using the life history trait PC scores for axes 1-3 within each grid cell (*47*). The convex-hull volume is a widely used method to test for macroevolutionary signatures of trait diversity and habitat filtering (*47*). To avoid known effects of variable plot sizes between North and South America (see table S1) and minimize the potential effects of local scale disturbance events on broadscale diversity patterns, we balanced the number of individual tree observations across our biogeographic gradient (see materials and methods, section 1) and calculated the convex hull volume across equal sized hexagon grids. Four of our grid cells did not meet the minimum number of species that were needed to calculate the convex-hull volume (i.e., included < 4) and were thus excluded from our analysis.

The convex hull volume of each grid cell was then used to test for predictable variation in demographic trait diversity across biogeographic gradients, using a generalized linear model (Fig 1c, H3). We used mean annual temperature as our predictor variable because it was found to have the strongest effect on our univariate traits (see Figs. 3 and S9). We also tested for two non-mutually exclusive expectations of a positive relationship between demographic diversity and ecosystem productivity, including the expectation from an evolutionary theory perspective (i.e., productivity should drive diversification) and functional perspective (i.e., more diverse systems should be more productive). To test these non-mutually exclusive hypotheses (Fig 1c, H3), we used linear and generalized linear models. The predictor variables were scaled to a mean of zero and a standard deviation of one. We assessed the normality of the residuals and, when needed, we transformed the variable by the natural log. It is important to note that mean annual temperature and our remotely sensed estimate of above-ground net primary productivity (NPP) were based on multi-year mean conditions from 1997-2013 (*48*). These multi-year averages serve as coarse proxies of the conditions related to the mean pace of life for trees over the last century (life expectancies, etc.), which were derived from dynamical data collected from 1926 to 2014.

Supplementary Figures:

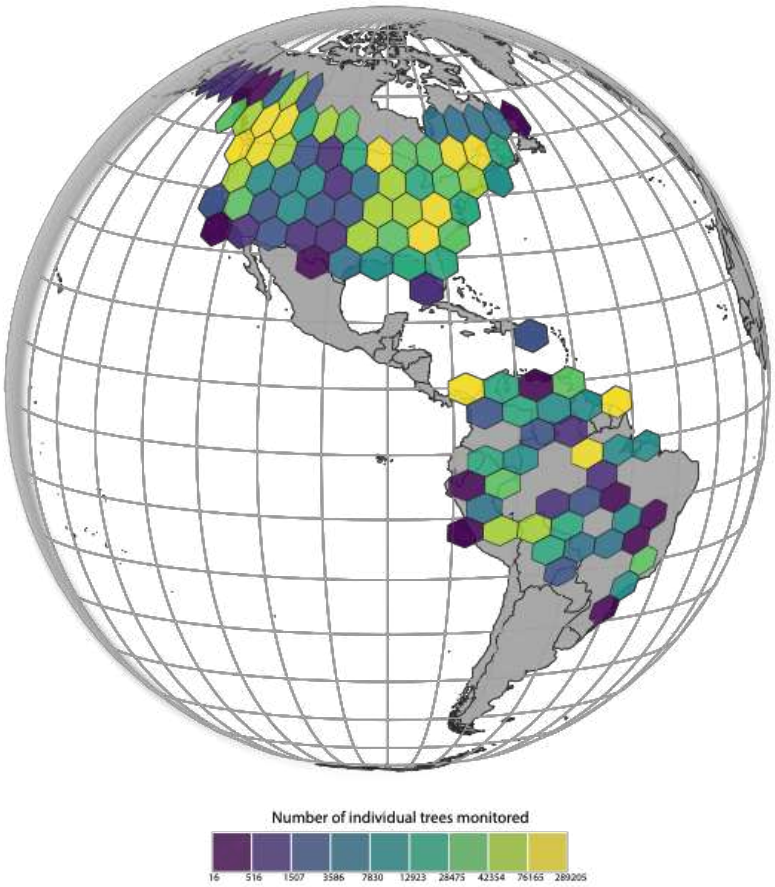

Figure S1. Map of equal area hexagon grids (size ~ 250,000 km^2) that were used to calculate our species by grid ID life history traits. The heatmap represents the total number of tree observations within each grid cell.

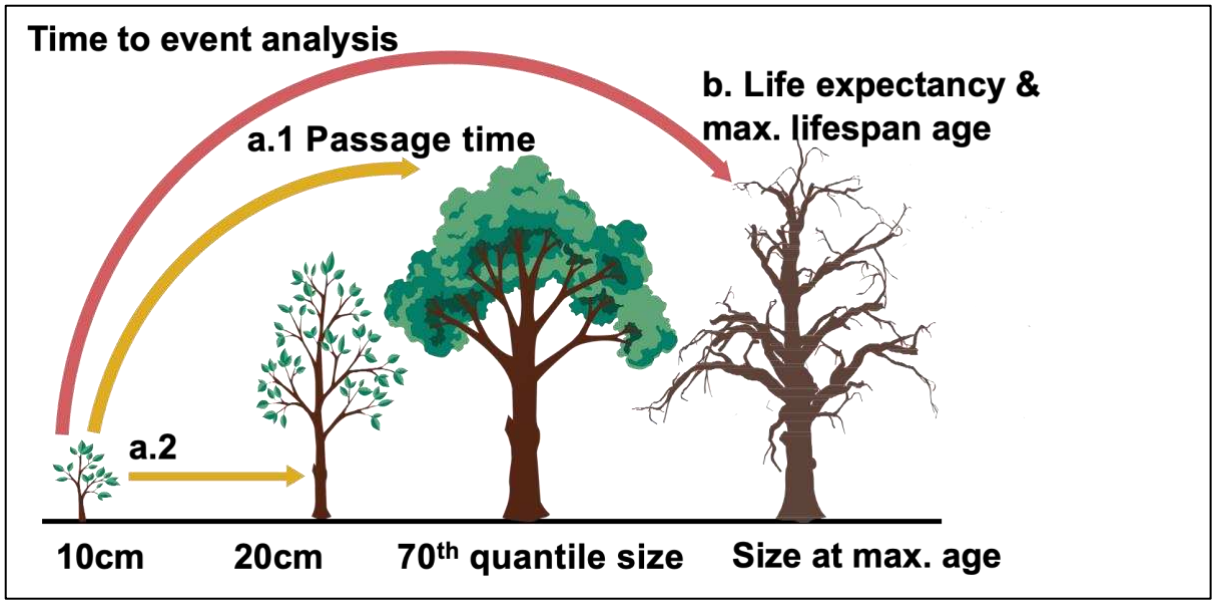

Figure S2. Visual illustration of life-history traits, including first passage times from 10 to 20 cm dbh and the 70% quantile of the observed size distribution, the life expectancy from 10 cm dbh, and the maximal lifespan age and size.

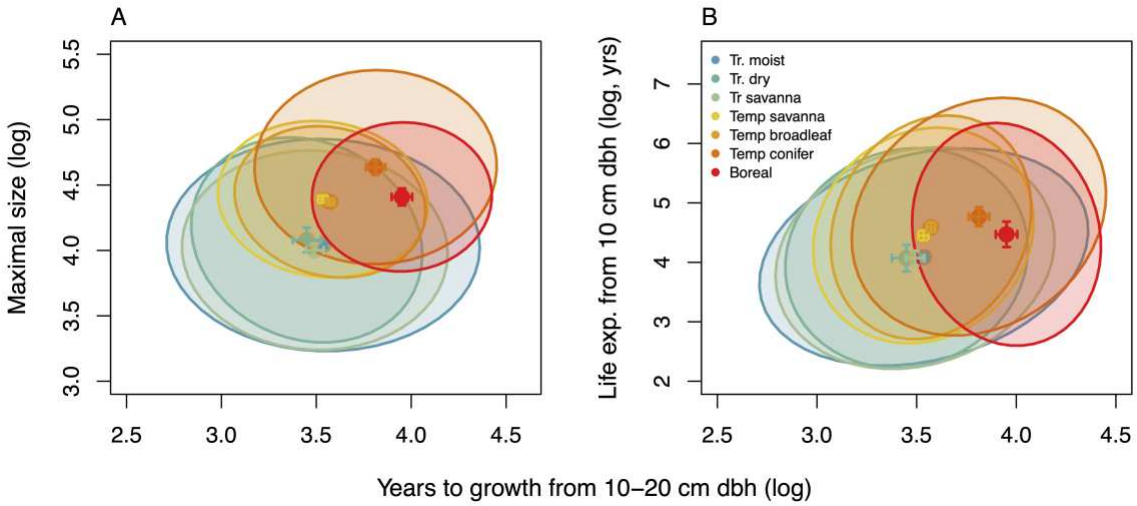

Figure S3. The relationship between growth-longevity-stature relationships across forest biomes, with means and 95% CI values. Ellipses capture the 70th quartile of trait variation among biomes (i.e., range of life history trait occupied by species across biomes.

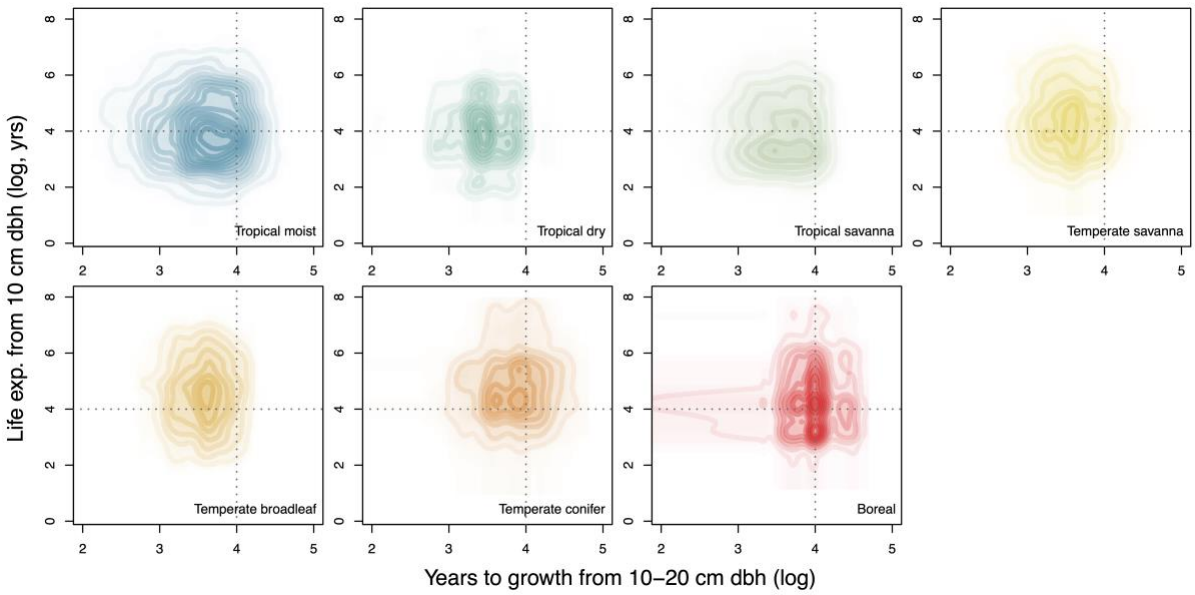

Figure S4. Heatmaps across biomes that show the relationship between tree growth strategies and the remaining life expectancies from 10 cm dbh. Color transparency represents the concentration of species with similar trait values, with less transparent colors representing a high concentration of species with similar trait values within biome.

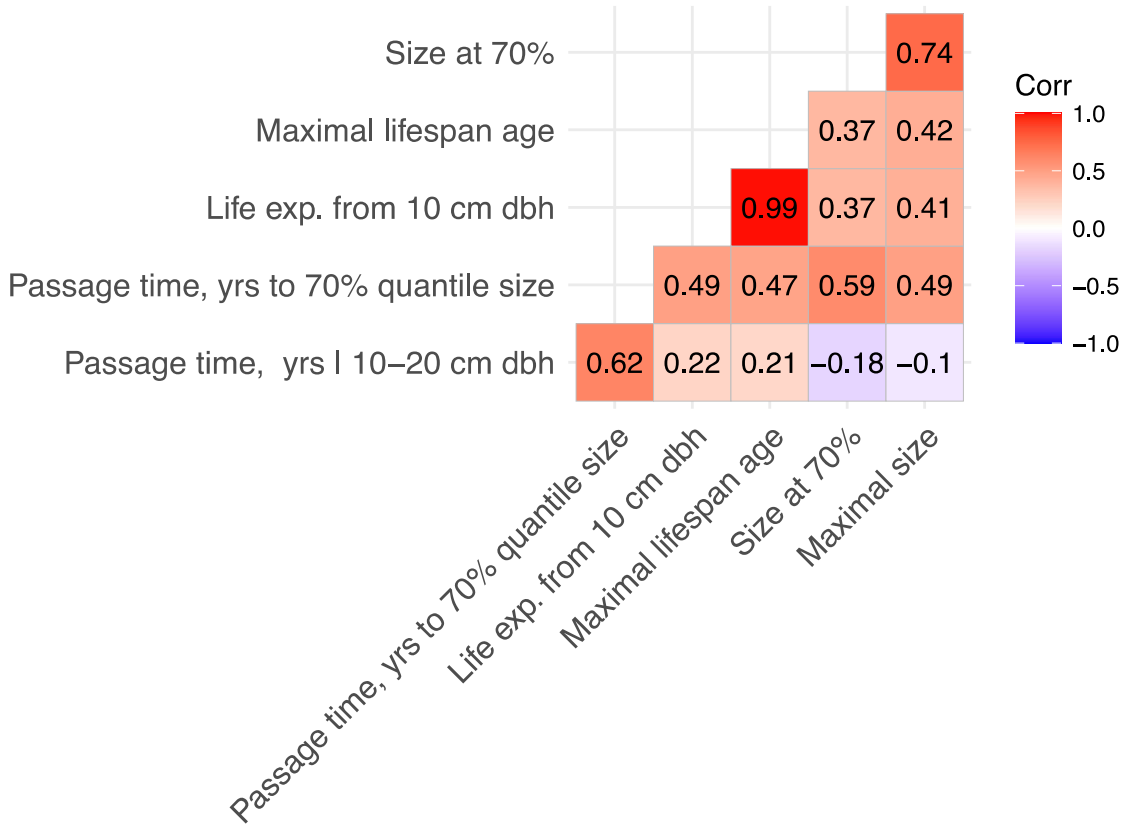

Figure S5. Life history trait correlations.

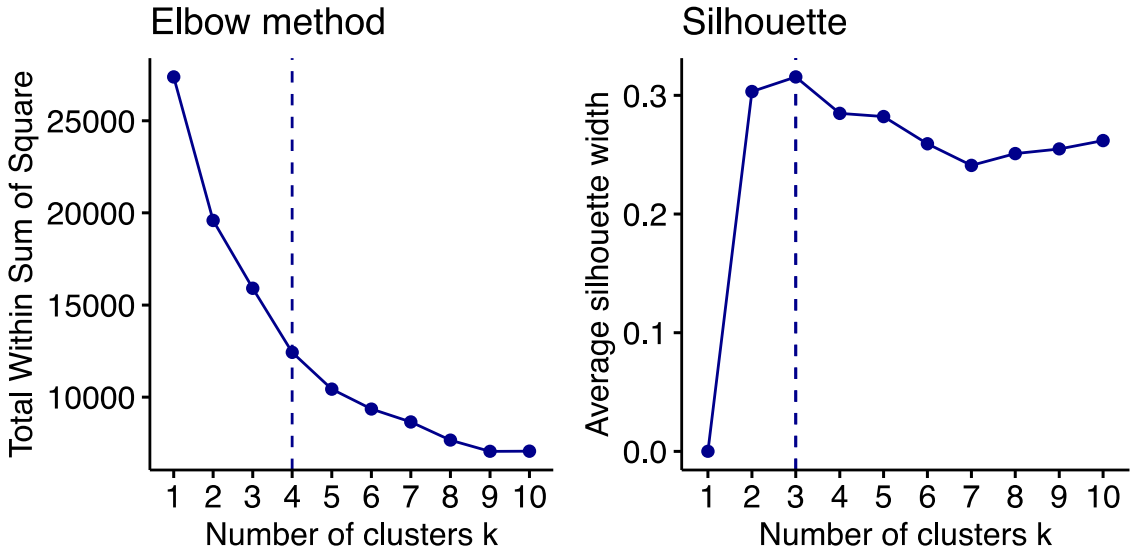

Figure S6. Optimal number of clusters using the elbow total within sum of square and Silhouette methods, including all species.

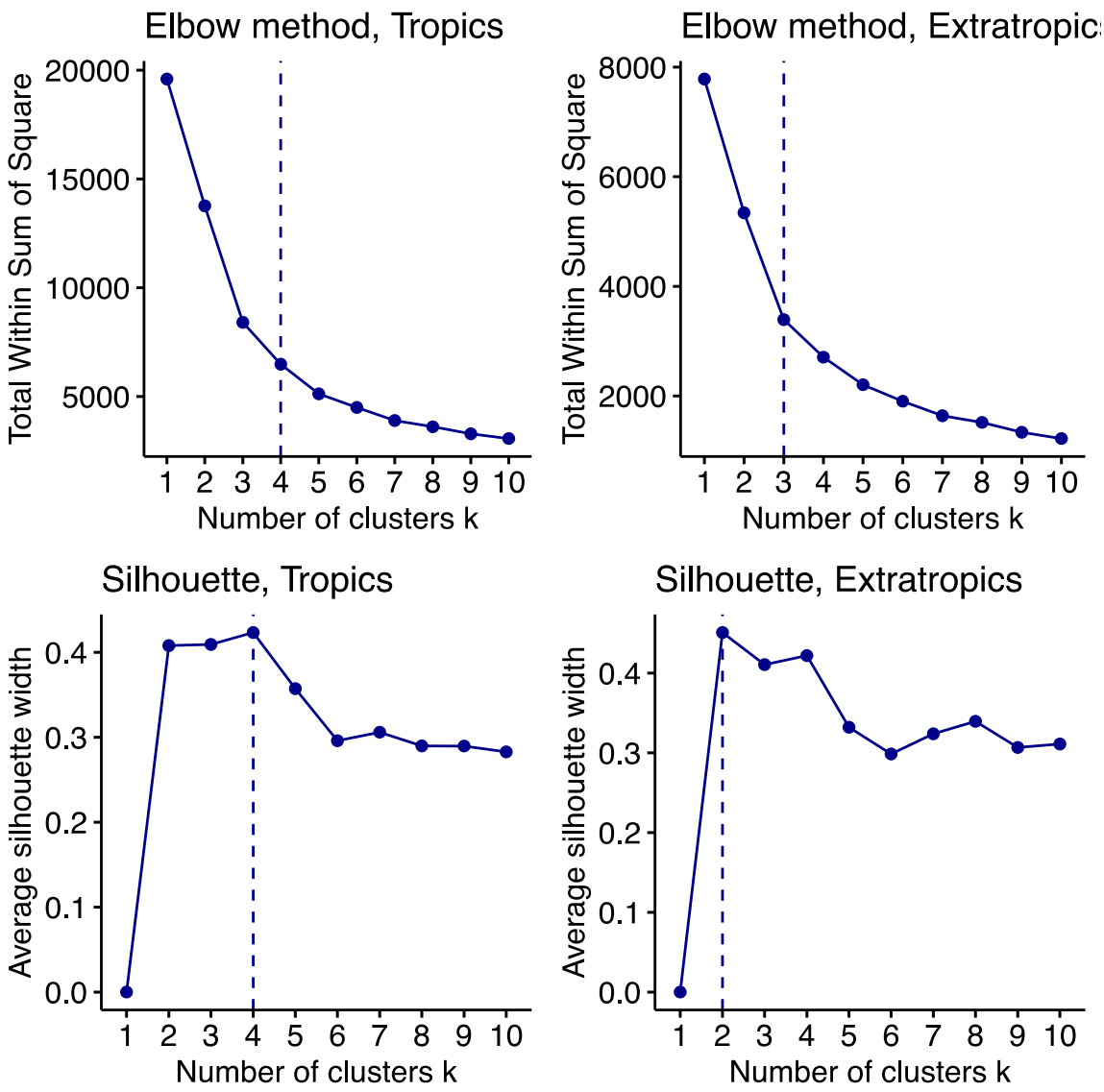

Figure S7. Optimal number of clusters using the elbow total within sum of square and silhouette methods for species in the tropics and extratropics.

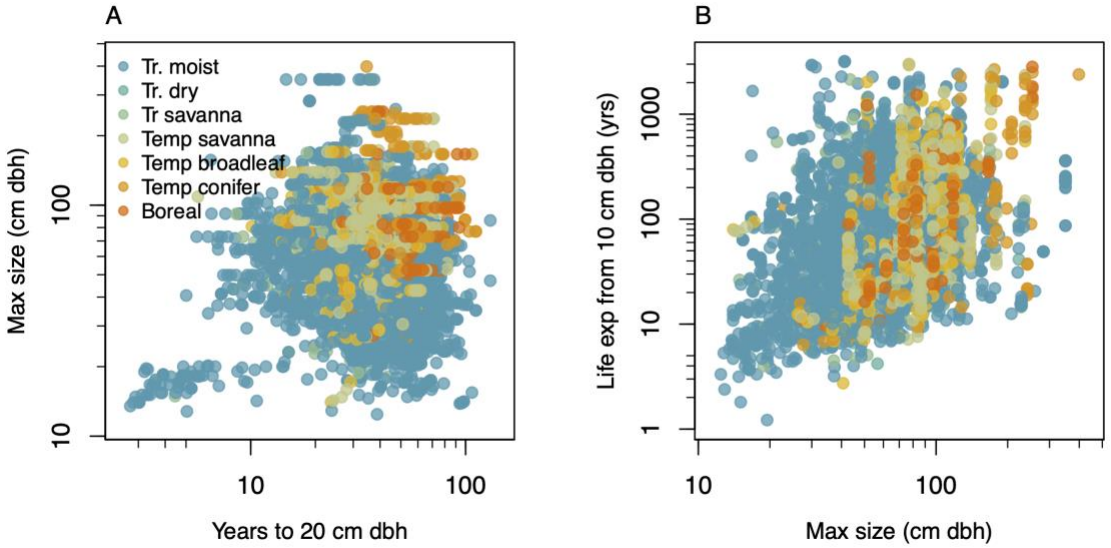

Figure S8. Visual illustration of tree growth- longevity-stature relationships for all species within each grid cell (total of 1,127 species and 6,847 trait values, i.e., species × grid).

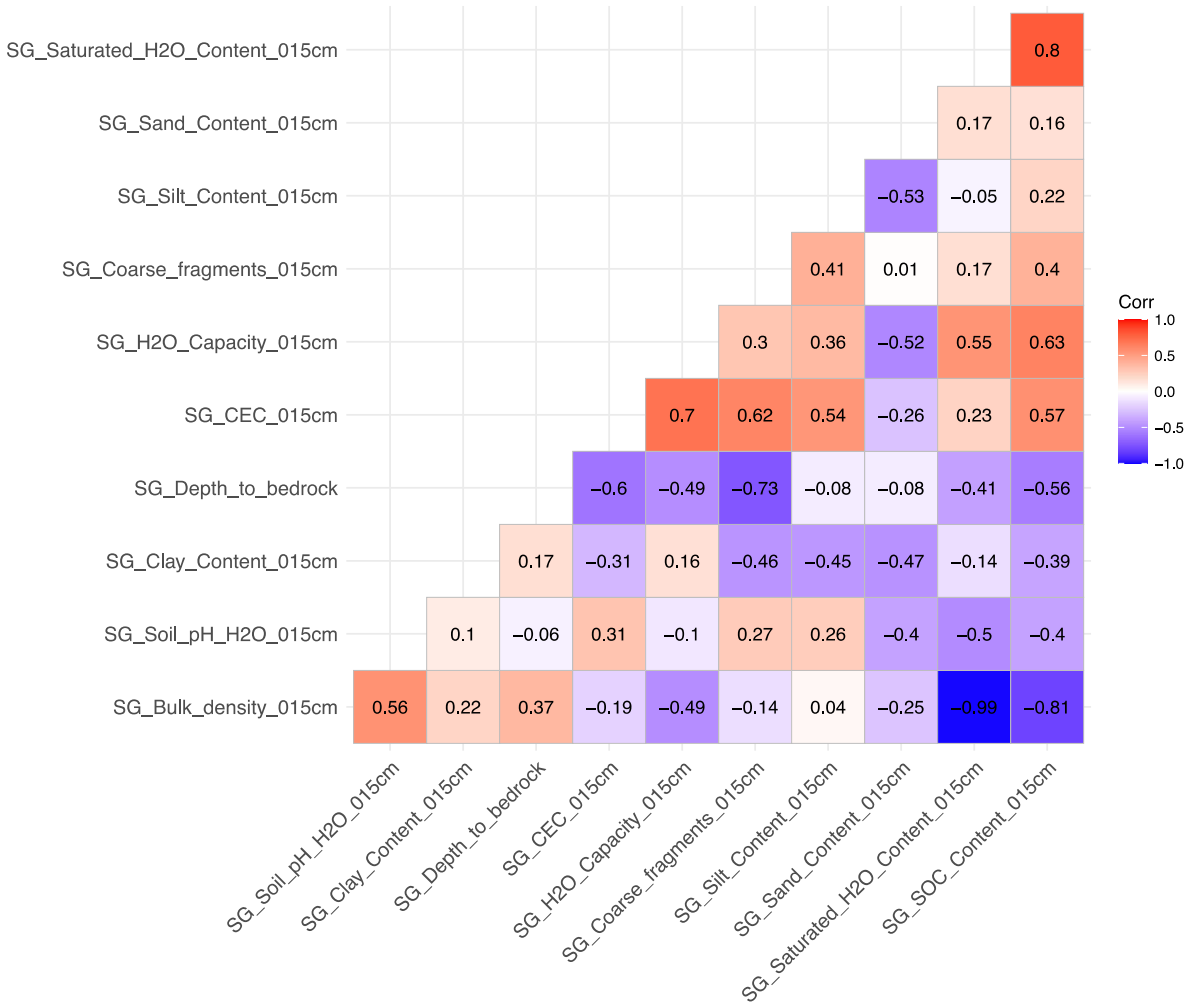

Figure S9. Correlations among soil variables, extracted from soil grids (GS)(*64*).

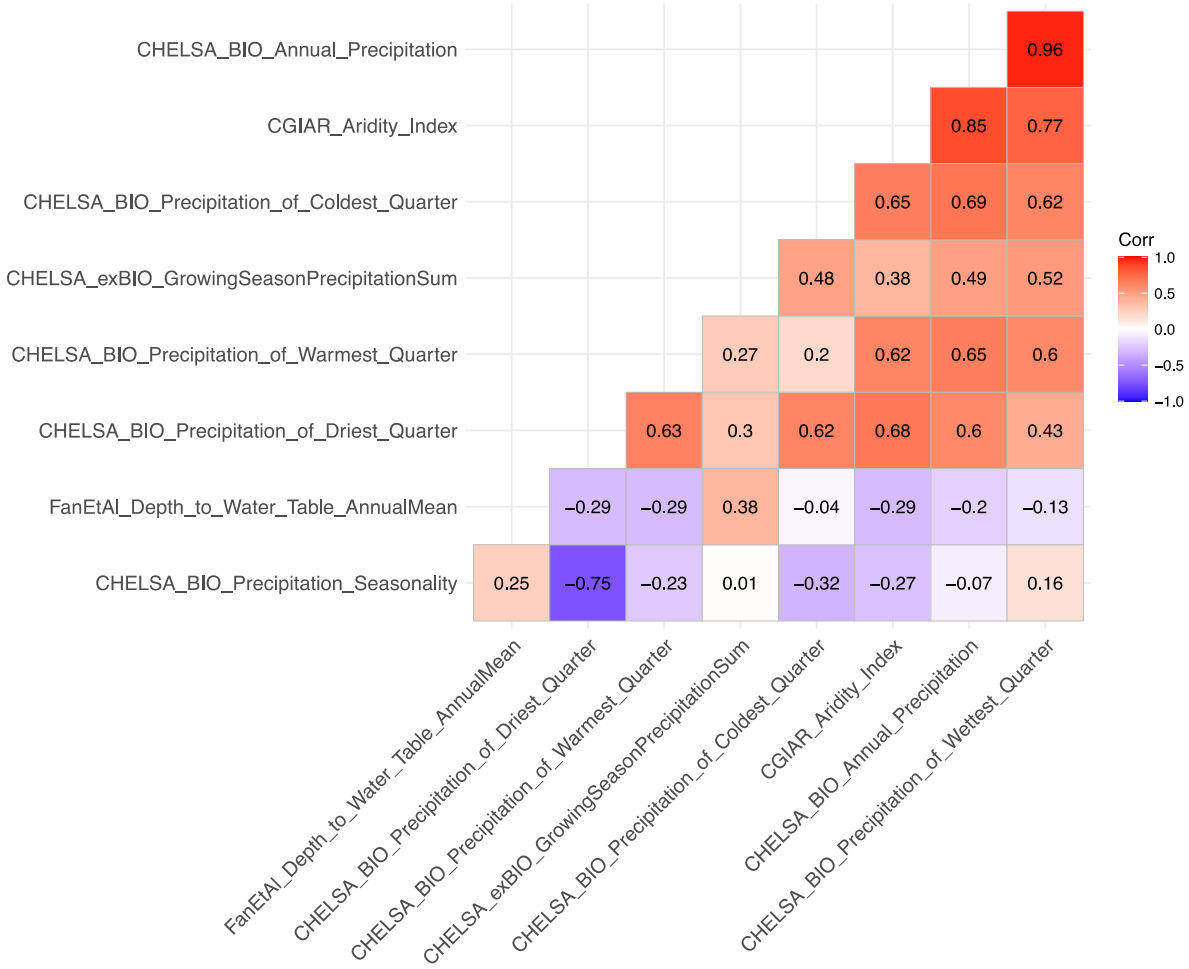

Figure S10. Correlations among precipitation variables.

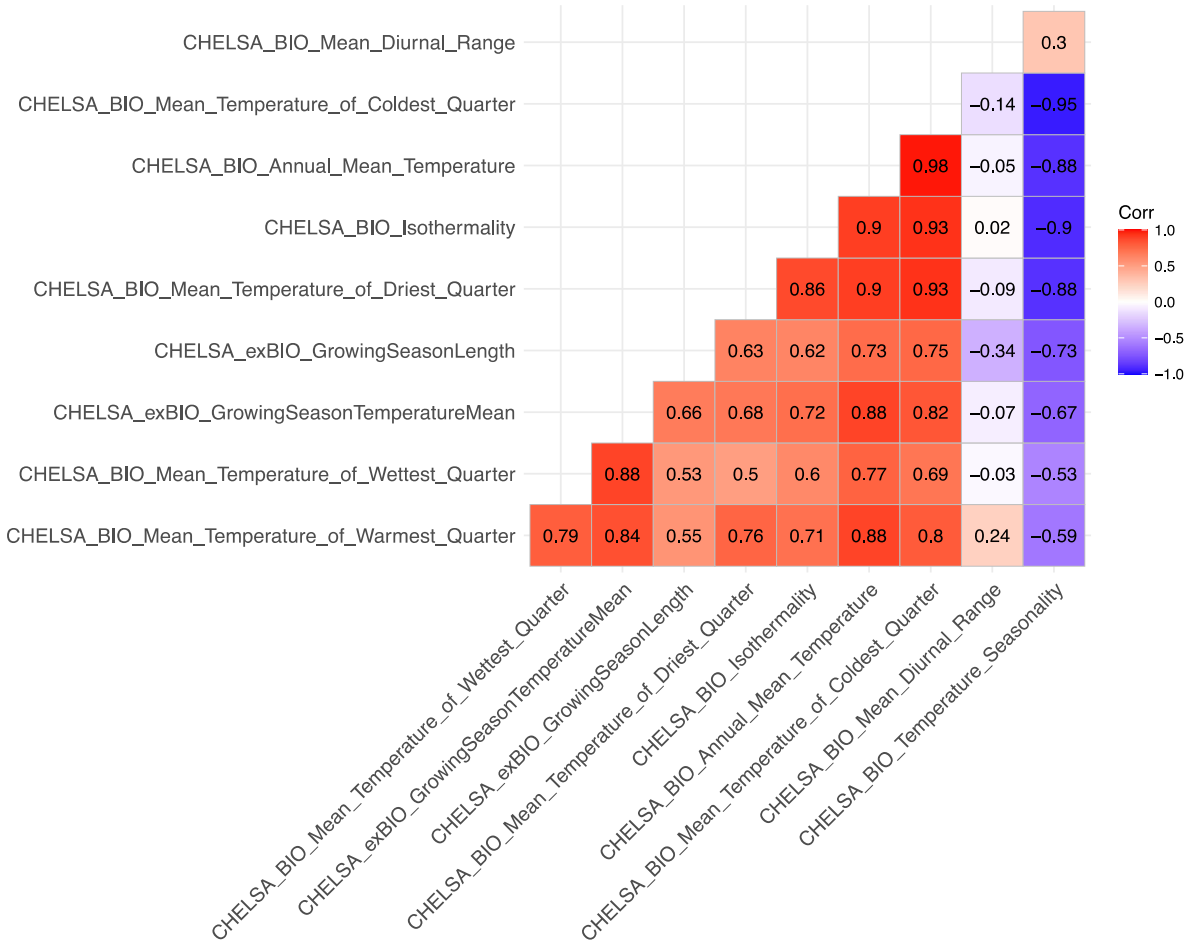

Figure S11. Correlations among temperature variables.

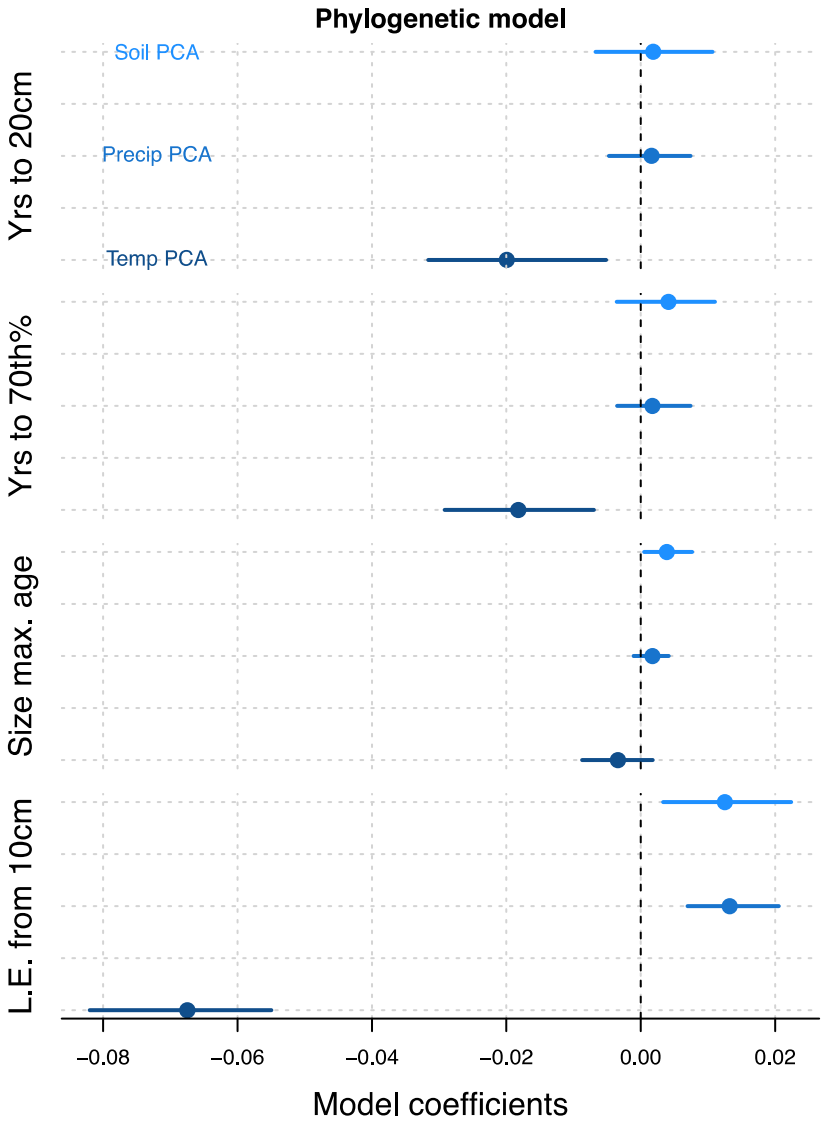

Figure S12. Estimated coefficients, with posterior mean and 95% credible intervals, for life history traits across broadscale soil, temperature, and precipitation gradients, using a multi-response Bayesian generalized mixed effect model.

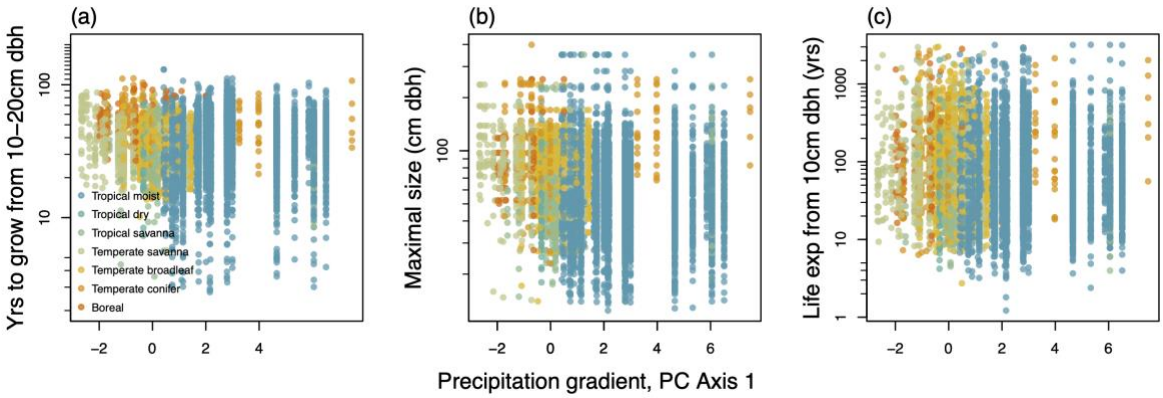

Figure S13. Life history trait variation across a precipitation gradient, which represents the first PC axis of 8 precipitation variables that we derived from WorldClim(*48*) and SoilGrids and span a latitudinal gradient from southern Brazil to northern Canada. The Y-axis is scaled by the natural log. Data points are species- and grid-specific and are calculated using individual tree observations to fit size-based integral projection models for each species within each grid cell ID. Model coefficients of the multi-response Bayesian model are reported in Fig. SI.10).

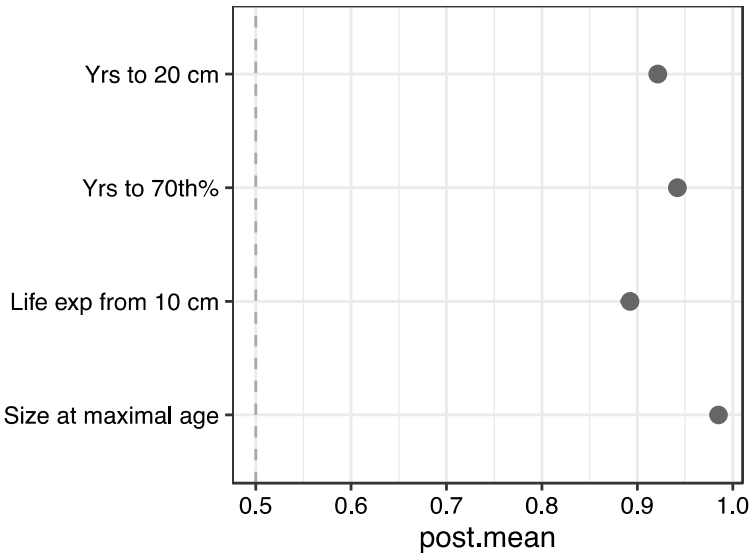

Figure S14. Estimated phylogenetic heritability from the Bayesian multiple-response mixed effect model, with posterior mean and 95% credible intervals.

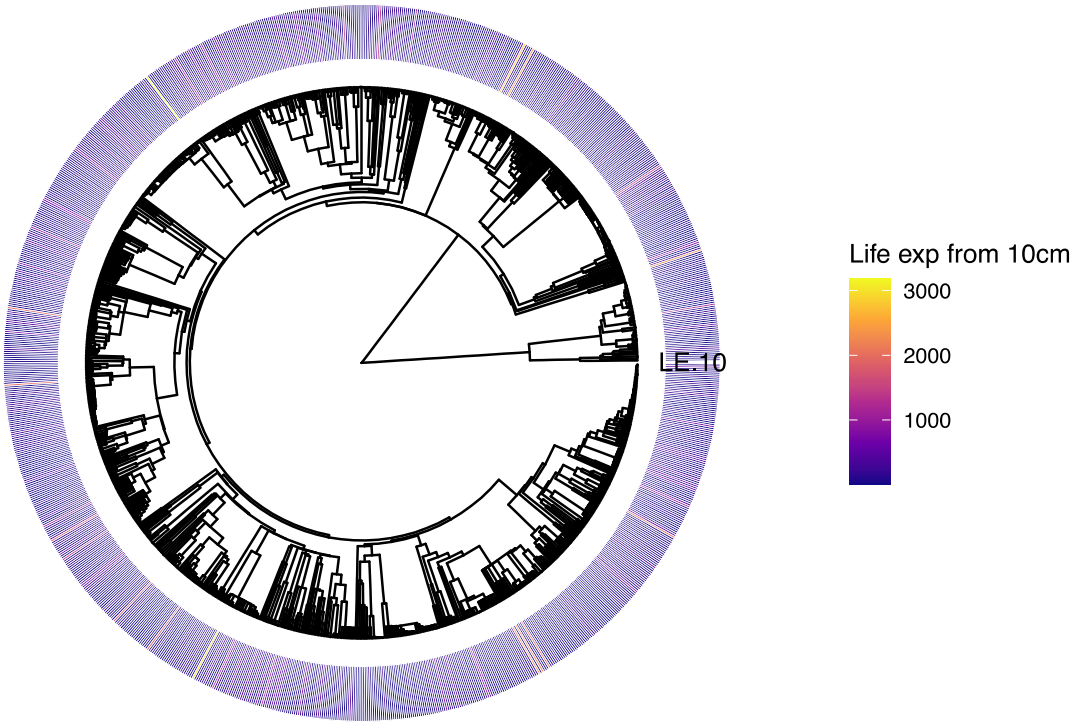

Figure S15. The phylogenetic tree for species included in our study, with a heatmap of tree life expectancies from 10 cm dbh.

Supplementary Tables:

S1. Forest inventory network datasets used in this study.

Network name	Network regional code	# of unique tree measurements	# of species	Min census year	Max census year	Countries
ForestGeo	FGE	180,002	216	1982	2013	Panama and United States of America
ForestPlots	FPN	633,406	921	1961	2013	Bolivia, Brazil, Colombia, Ecuador, French Guiana, Guyana, Peru, Suriname, Venezuela
NFI	NAL	313,091	13	1960	2007	Canada (Alberta)
NFI	NBC	702,018	28	1926	2012	Canada (British Columbia)
NFI	NQU	252,176	34	1970	2014	Canada (Quebec)
NFI	NSA	84,207	9	1958	1999	Canada (Saskatchewan)
SYN	SYN	24,070	13	1982	2014	United States of America
FIA	FIAN	303,264	130	1999	2013	United States of America
FIA	FIANE	170,424	102	2001	2013	United States of America
FIA	FIANW	96,804	52	1995	2007	United States of America
FIA	FIARM	63,917	30	2000	2008	United States of America
FIA	FIAS	374,777	154	2000	2013	United States of America

Table S2. Mean and CI values in the number of years it takes trees to go to 20 cm in diameter across biomes. The history-history traits were scaled by the natural log before calculating the mean traits and back-transformed for reporting peruses.

Life expectancy from 10 cm in diameter						
Biome	**Min.**	**1st Qu.**	**Median**	**Mean**	**3rd Qu.**	**Max.**
Boreal	10	35	73	87	186	2825
Temperate conifer	6	48	108	118	245	2674
Temperate broadleaf	3	39	100	98	253	3005
Temperate savanna	7	36	79	86	189	2976
Tropical dry	4	27	54	59	112	2037
Tropical moist	1	25	54	60	129	3195
Tropical savanna	4	23	56	59	129	2143

Growth strategy, years to grow from 10-20 cm in diameter						
Biome	**Min.**	**1st Qu.**	**Median**	**Mean**	**3rd Qu.**	**Max.**
Boreal	27	42	53	52	62	99
Temperate conifer	14	35	48	45	61	112
Temperate broadleaf	10	29	36	36	45	83
Temperate savanna	4	25	35	33	46	85
Tropical dry	7	26	32	31	41	82
Tropical moist	3	26	37	34	50	130
Tropical savanna	4	25	35	33	46	85

S3. Principal component analysis loadings of the life history traits.

ALL species	**PC 1**	**PC 2**	**PC 3**	**PC 4**
Yrs to 20 cm dbh	0.513	0.616	0.12	0.585
Yrs to 70th max size	0.68	0.129	-0.227	-0.685
Life exp. From 10 cm dbh	0.344	-0.433	0.833	
Max size	0.395	-0.645	-0.49	0.433

Tropical species				
Yrs to 20 cm dbh	0.55	0.591		0.586
Yrs to 70th max size	0.702		0.216	-0.679
Life exp. From 10 cm dbh	0.306	-0.214	-0.928	
Max size	0.333	-0.777	0.299	0.442

Extratropical species				
Yrs to 20 cm dbh	0.481	0.603	0.227	0.594
Yrs to 70th max size	0.64	0.252	-0.192	-0.7
Life exp. From 10 cm dbh	0.388	-0.545	0.742	
Max size	0.456	-0.526	-0.601	0.393

S4. List of the environmental variables included in the soil, temperature, and precipitation variables used in the multi-response Bayesian generalized mixed effect model.

Env. group	Variable name	Data source	Unit	Resolution
Soil	Bulk density 015cm	Soilgrids(*64*)		≈250m
Soil	Soil pH H2O 15cm	Soilgrids(*64*)		≈250m
Soil	Clay content 15cm	Soilgrids(*64*)		≈250m
Soil	Saturated H2O content 15cm	Soilgrids(*64*)		≈250m
Soil	Silt content 15cm	Soilgrids(*64*)		≈250m
Soil	CEC 15cm	Soilgrids(*64*)		≈250m
Soil	SOC content 15cm	Soilgrids(*64*)		≈250m
Soil	Sand content 15cm	Soilgrids(*64*)		≈250m
Soil	Coarse fragments 15cm	Soilgrids(*64*)		≈250m
Soil	Depth to bedrock	Soilgrids(*64*)		≈250m
Soil	H2O capacity 15cm	Soilgrids(*64*)		≈250m
Soil	Sand content 15cm	Soilgrids(*64*)		≈250m
Precipitation	Aridity index	CGIAR (*48*)	AI value	1km
Precipitation	Annual precipitation	CHELSA(*68*)	mm	30 arcsec (≈900m at equator)
Precipitation	Precipitation of coldest quarter	CHELSA(*68*)	mm	30 arcsec (≈900m at equator)
Precipitation	Precipitation of driest quarter	CHELSA(*68*)	mm	30 arcsec (≈900m at equator)
Precipitation	Precipitation of warmest quarter	CHELSA(*68*)	mm	30 arcsec (≈900m at equator)
Precipitation	Precipitation of wettest quarter	CHELSA(*68*)	mm	30 arcsec (≈900m at equator)
Precipitation	Precipitation seasonality	CHELSA(*68*)	mm	30 arcsec (≈900m at equator)
Precipitation	Growing season precipitation sum	CHELSA(*68*)	mm	30 arcsec (≈900m at equator)
Precipitation	Depth to water table annual mean	CHELSA(*68*)	mm	30 arcsec (≈900m at equator)
Temperature	Isothermality	CHELSA(*68*)	Unitless	30 arcsec (≈900m at equator)

Temperature	Mean diurnal range	CHELSA(*68*)	°C	30 arcsec (≈900m at equator)
Temperature	Mean temperature of coldest quarter	CHELSA	°C	30 arcsec (≈900m at equator)
Temperature	Mean temperature of coldest quarter	CHELSA	°C	30 arcsec (≈900m at equator)
Temperature	Mean temperature of coldest quarter	CHELSA	°C	30 arcsec (≈900m at equator)
Temperature	Mean temperature of coldest quarter	CHELSA	°C	30 arcsec (≈900m at equator)
Temperature	Temperature seasonality	CHELSA	°C	30 arcsec (≈900m at equator)
Temperature	Growing season length	CHELSA	Number of days	30 arcsec (≈900m at equator)
Temperature	Growing season temperature mean	CHELSA	°C	30 arcsec (≈900m at equator)

Table S5. Results of Bayesian generalized mixed effect model, with estimates of posterior means, upper and lower credible intervals.

Life history trait	Env. variable	post.mean	lower-95% CI	upper-95% CI	eff.samp	p value MCMC	
Life exp. From 10 cm dbh	--	0.055	-0.030	0.134	1000.0	0.218	
Yrs to 20 cm dbh	--	0.160	0.082	0.256	1000.0	0.001	**
Yrs to 70th max size	--	0.106	0.022	0.193	1000.0	0.020	*
Max size	--	-0.273	-0.357	-0.191	1000.0	0.001	***
Life exp. From 10 cm dbh	Soil PCA	0.012	0.003	0.022	1115.9	0.016	*
Yrs to 20 cm dbh	Soil PCA	0.002	-0.007	0.011	1000.0	0.686	
Yrs to 70th max size	Soil PCA	0.004	-0.004	0.011	1000.0	0.316	
Max size	Soil PCA	0.004	0.000	0.008	1117.3	0.040	*
Life exp. From 10 cm dbh	Precipitation PCA	0.013	0.007	0.021	1000.0	0.001	**
Yrs to 20 cm dbh	Precipitation PCA	0.002	-0.005	0.007	1000.0	0.620	
Yrs to 70th max size	Precipitation PCA	0.002	-0.004	0.007	1000.0	0.544	
Max size	Precipitation PCA	0.002	-0.001	0.004	1000.0	0.196	
Life exp. From 10 cm dbh	Temperature PCA	-0.067	-0.082	-0.055	1000.0	0.001	***
Yrs to 20 cm dbh	Temperature PCA	-0.020	-0.032	-0.005	1000.0	0.002	**
Yrs to 70th max size	Temperature PCA	-0.018	-0.029	-0.007	1000.0	0.002	**
Max size	Temperature PCA	-0.003	-0.009	0.002	1000.0	0.200	

Signif. codes: 0 ‘***’ 0.001 ‘**’ 0.01 ‘*’ 0.05 ‘.’ 0.1 ‘ ’ 1

Table S6. Phylogenetic variance-covariance of the Bayesian generalized mixed effect model, with the genetic and residual correlations for each life history trait and Pagel's lambda.

Phenotypic correlations [variance-covariance of standardized traits]

	Life exp. From 10 cm dbh	Yrs to 20 cm dbh	yrs to 70th max size	Max size
Life exp. From 10 cm dbh	1	0.18	0.32	0.34
Yrs to 20 cm dbh	0.18	1	0.61	-0.04
Yrs to 70th max size	0.32	0.61	1	0.41
Max size	0.34	-0.04	0.41	1

Genetic variance-covariance

	Life exp. From 10 cm dbh	Yrs to 20 cm dbh	yrs to 70th max size	Max size
Life exp. From 10 cm dbh	0.94	0.21	0.36	0.35
Yrs to 20 cm dbh	0.21	1.14	0.67	-0.05
Yrs to 70th max size	0.36	0.67	1.15	0.48
Max size	0.35	-0.05	0.48	1.09

Residual variance-covariance

	Life exp. From 10 cm dbh	Yrs to 20 cm dbh	yrs to 70th max size	Max size
Life exp. From 10 cm dbh	0.12	0.00	0.00	0.01
Yrs to 20 cm dbh	0.00	0.10	0.08	0.00
Yrs to 70th max size	0.00	0.08	0.07	0.00
Max size	0.01	0.00	0.00	0.02

Genetic correlations

	Life exp. From 10 cm dbh	Yrs to 20 cm dbh	yrs to 70th max size	Max size
Life exp. From 10 cm dbh	1	0.20	0.35	0.35
Yrs to 20 cm dbh	0.20	1	0.59	-0.05
Yrs to 70th max size	0.35	0.59	1	0.43
Max size	0.35	-0.05	0.43	1

Residual correlations

	Life exp. From 10 cm dbh	Yrs to 20 cm dbh	yrs to 70th max size	Max size
Life exp. From 10 cm dbh	1	-0.04	-0.01	0.28
Yrs to 20 cm dbh	-0.04	1	0.93	0.08
Yrs to 70th max size	-0.01	0.93	1	0.08
Max size	0.28	0.08	0.08	1

Pagel's lambda

	lambda	Lower CI	Upper CI
Life exp. From 10 cm dbh	0.89	0.88	0.90
Yrs to 20 cm dbh	0.92	0.92	0.93
Yrs to 70th max size	0.94	0.94	0.95
Max size	0.99	0.98	0.99

Table S7. Linear model coefficients and summary statistics associated with Fig 4, including species richness and demographic trait diversity (**A**), mean annual temperature and demographic trait diversity (**B**), net primary productivity and demographic trait diversity table (**C**), and the combined effect of demographic trait diversity and mean annual temperature on net primary productivity (**D**).

Species richness on demo. diversity (Fig 4.A)

Term	Estimate	Std error	Statistic	P value
(Intercept)	-6.732	0.984	-6.840	<0.01
Species richness (log)	2.193	0.554	3.959	0.000
Species.richness^2 (log)	-0.146	0.073	-2.006	0.048

Adj $R^2 = 0.65$, $F_{2,82} = 79$, $p < 0.01$

Mean annual temp on demo diversity (Fig 4.B)

Term	Estimate	Std error	Statistic	P value
(Intercept)	-2.267	0.2376	-9.541	<0.01
Mean annual temp (scaled)	0.106	0.0139	7.593	<0.01

Adj $R^2 = 0.40$, $F_{1,83} = 58$, $p < 0.01$

NPP on demo diversity (Fig 4.C)

Term	Estimate	Std error	Statistic	P value
NPP (scaled and log)	0.708	0.077	9.182	<0.01

Adj $R^2 = 0.49$, $F_{1,84} = 84.32$, $p < 0.01$

Demographic diversity on NPP (Fig 4.D)

Term	Estimate	Std error	Statistic	P value
Demo. diversity (scaled and log)	0.178	0.0441	4.041	<0.01
Mean annual temp. (scaled and log)	0.827	0.044	18.777	<0.01

Adj $R^2 = 0.90$, $F_{2,83} = 394.9$, $p < 0.01$

The effect of demographic diversity on NPP, tropics

Term	Estimate	Std error	Statistic	P value
Temp (scaled)	0.308	0.152	2.030	0.051
Demo diversity (log and scaled)	0.412	0.152	2 .716	0.011

Adj $R^2 = 0.26$, $F_{2,31} = 6.912$, $p = 0.003$

The effect of demographic diversity on NPP, extra-tropics

Term	Estimate	Std error	Statistic	P value
Temp (scaled)	0.790	0.068	11.611	<0.001
Demo diversity (log and scaled)	0.199	0.068	2.917	0.005

Adj $R^2 = 0.840$, $F_{2,50} = 136.6$, $p < 0.01$

1263